

Supporting information

# Impact of Aryloxy Initiators on the Living and Immortal Polymerization of lactide

Love-Ese Chile,<sup>1,2</sup> Tannaz Ebrahimi,<sup>1,2</sup> Alan Wong,<sup>1</sup> Dinesh C. Aluthge,<sup>1</sup> Savvas G. Hatzikiriakos<sup>2</sup> and Parisa Mehrkhodavandi <sup>1\*</sup>

<sup>1</sup> Department of Chemistry, University of British Columbia, 2036 Main Mall, Vancouver, British Columbia, Canada; <sup>2</sup> Department of Chemical and Biological Engineering, University of British Columbia, Vancouver, BC, Canada.

## Contents

A. Characterization of complexes 1-6 in the solution state .....	2
B. Characterization of complexes 2-6 in the solid state .....	21
C. Living ring-opening polymerization of lactide using catalysts 1-5 .....	29
D. Chain-end fidelity .....	33
E. In situ living ring-opening polymerization data with catalysts 1-4 .....	34
F. Alkoxy-phenoxy exchange kinetics .....	37
G. Immortal ring-opening polymerization data .....	38

## A. Characterization of complexes 1-6 in the solution state

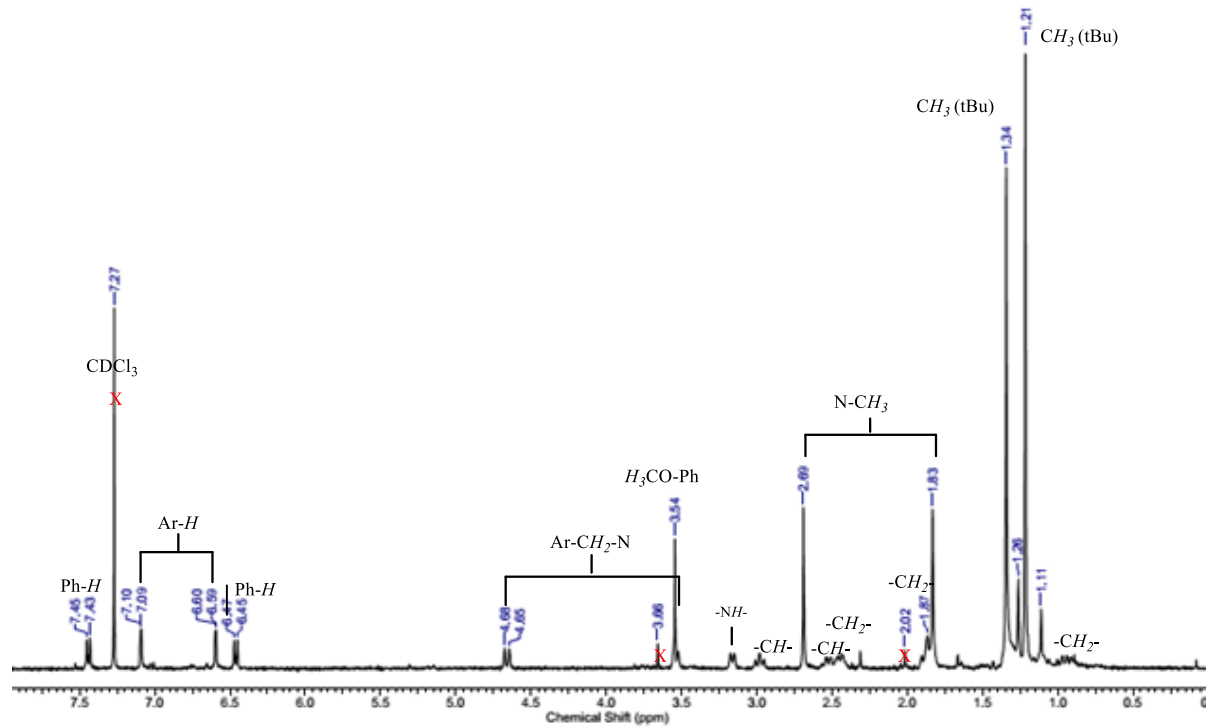


**Figure S1.**  $^1\text{H}$  NMR ( $\text{CDCl}_3$ , 25 °C) spectrum of  $(\pm)$ - $[ (\text{NNO})\text{InCl}]_2(\mu\text{-Cl})(\mu\text{-OPh}_{\text{OMe}})$  (**1**)

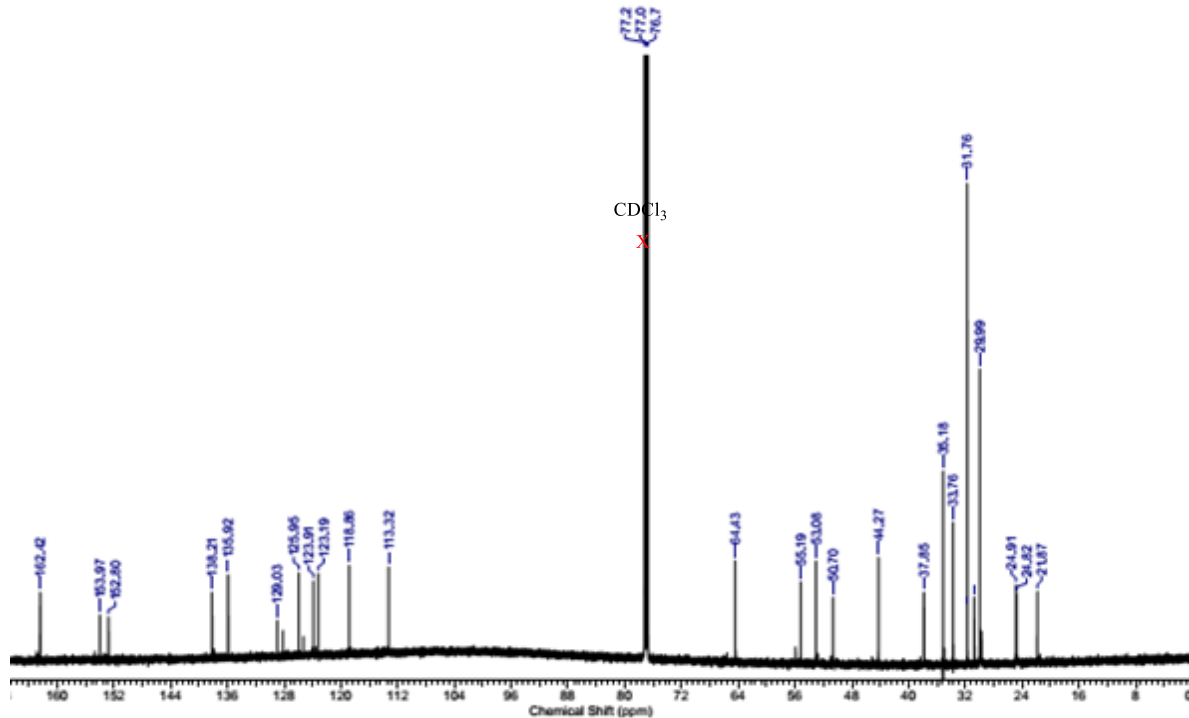


**Figure S2.**  $^{13}\text{C}\{^1\text{H}\}$  NMR ( $\text{CDCl}_3$ , 25 °C) spectrum of  $(\pm)$ - $[ (\text{NNO})\text{InCl}]_2(\mu\text{-Cl})(\mu\text{-OPh}_{\text{OMe}})$  (**1**)

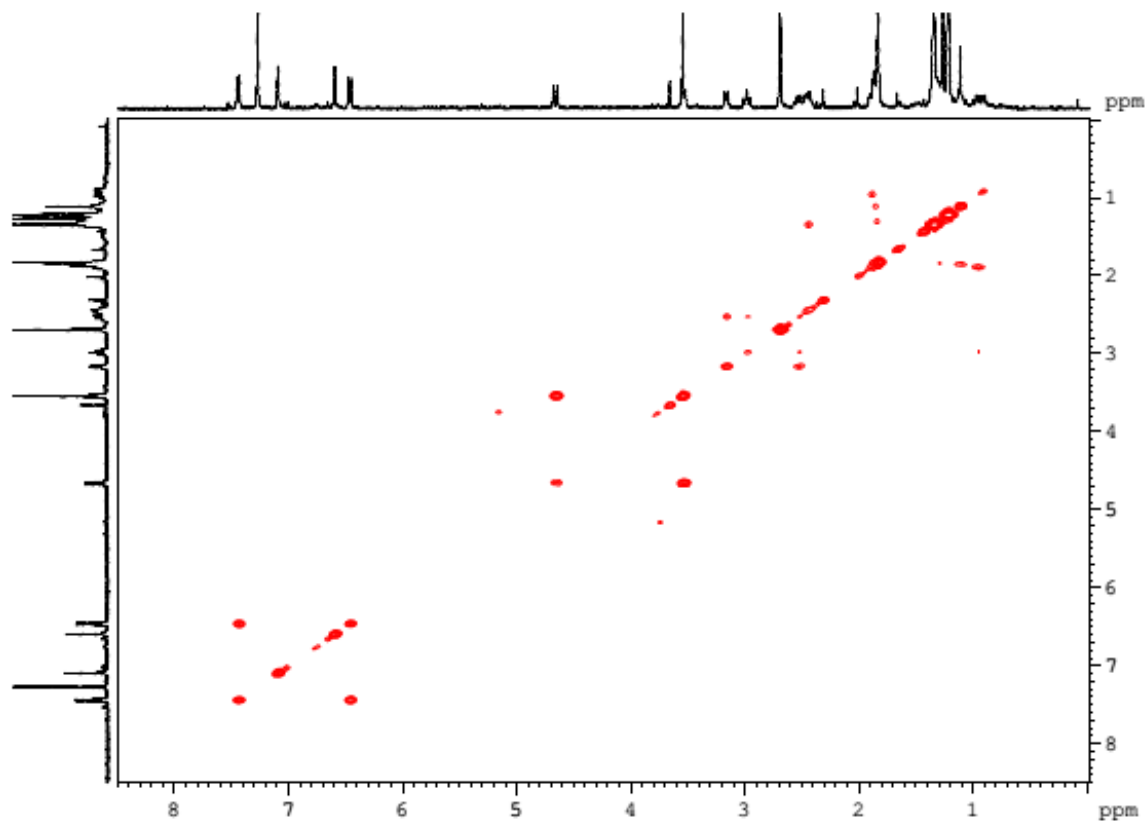


**Figure S3.**  $^1\text{H} - ^1\text{H}$  COSY ( $\text{CDCl}_3$ , 25 °C) spectrum of  $(\pm)$ - $[(\text{NNO})\text{InCl}]_2(\mu\text{-Cl})(\mu\text{-OPh}_{\text{OMe}})$  (**1**)

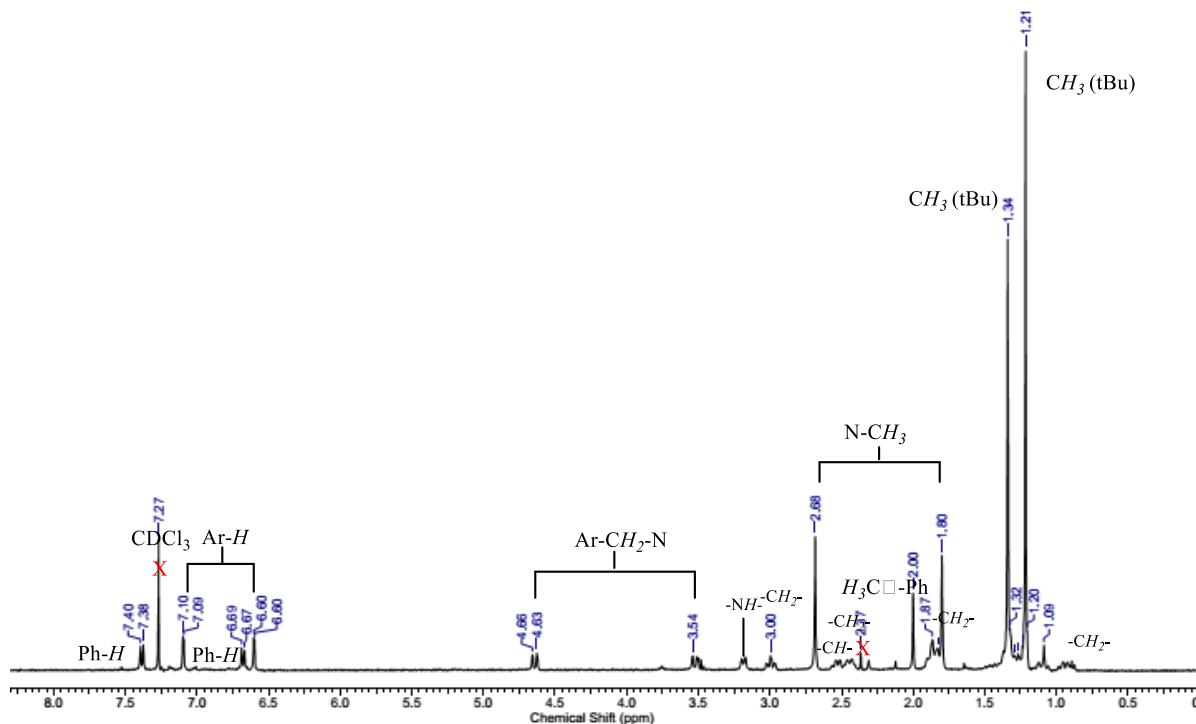


**Figure S4.** <sup>1</sup>H NMR (CDCl<sub>3</sub>, 25 °C) spectrum of (±)-[(NNO)InCl]<sub>2</sub>(μ-Cl)(μ-OPh<sub>Me</sub>) (**2**)

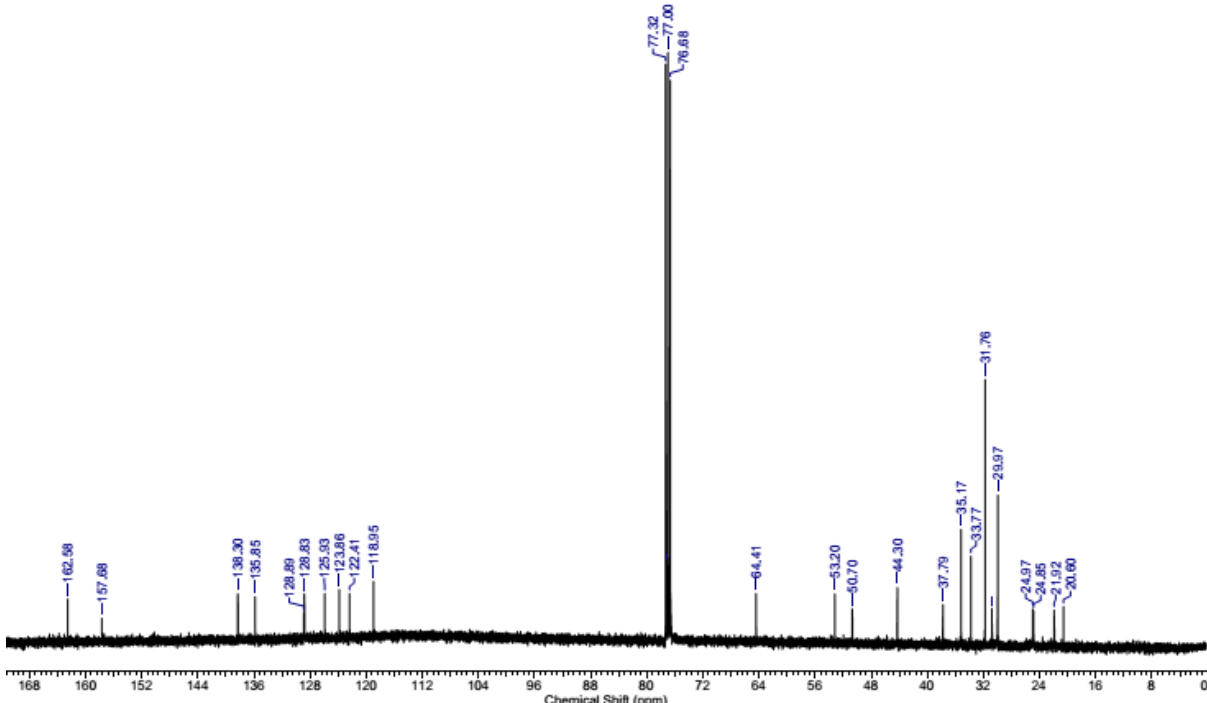


**Figure S5.** <sup>13</sup>C{<sup>1</sup>H} NMR (CDCl<sub>3</sub>, 25 °C) spectrum of (±)-[(NNO)InCl]<sub>2</sub>(μ-Cl)(μ-OPh<sub>Me</sub>) (**2**)

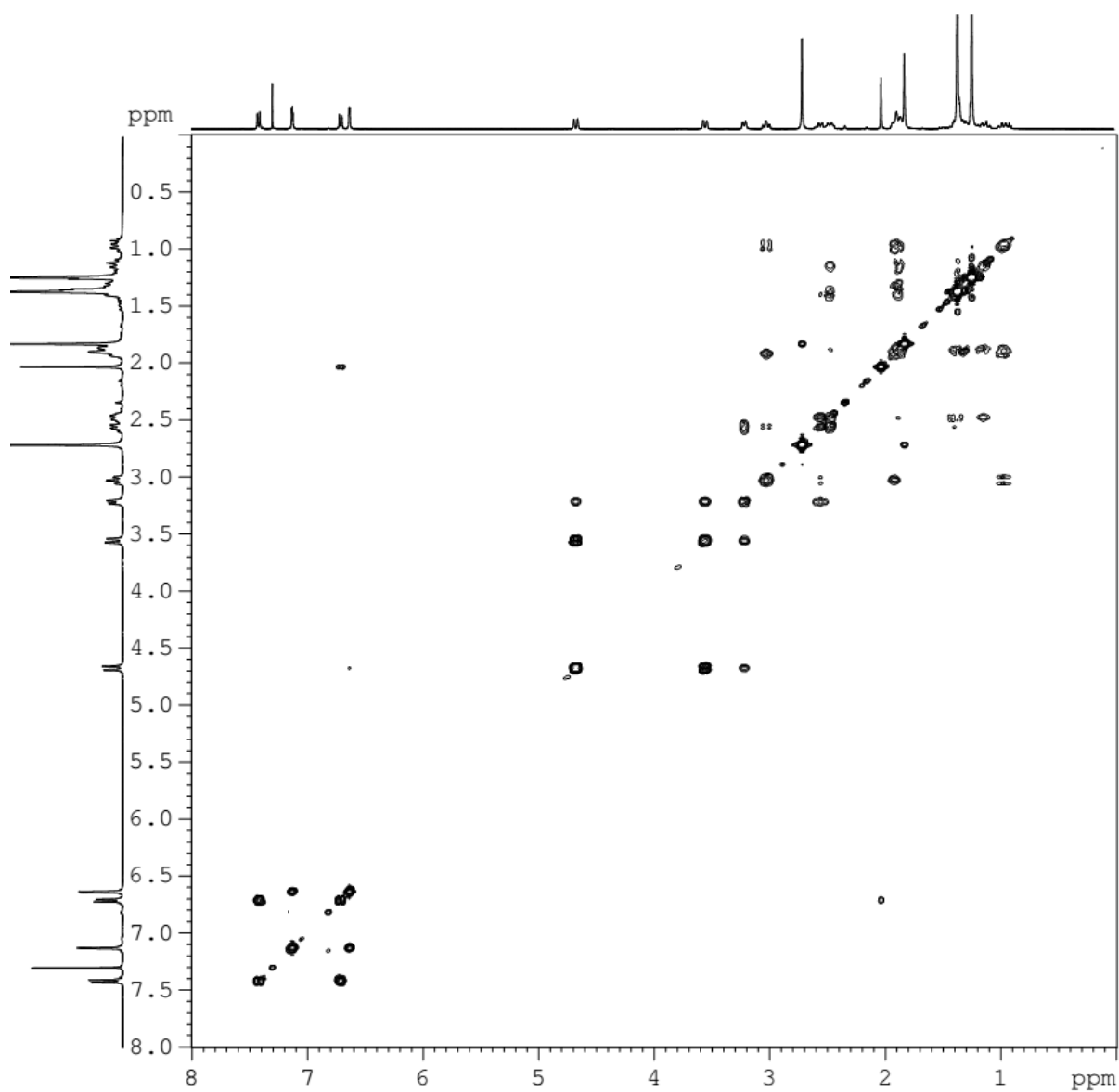


**Figure S6.**  $^1\text{H}$  -  $^1\text{H}$  COSY ( $\text{CDCl}_3$ , 25 °C) spectrum of  $(\pm)$ - $[(\text{NNO})\text{InCl}]_2(\mu\text{-Cl})(\mu\text{-OPh}_{\text{Me}})$  (2)

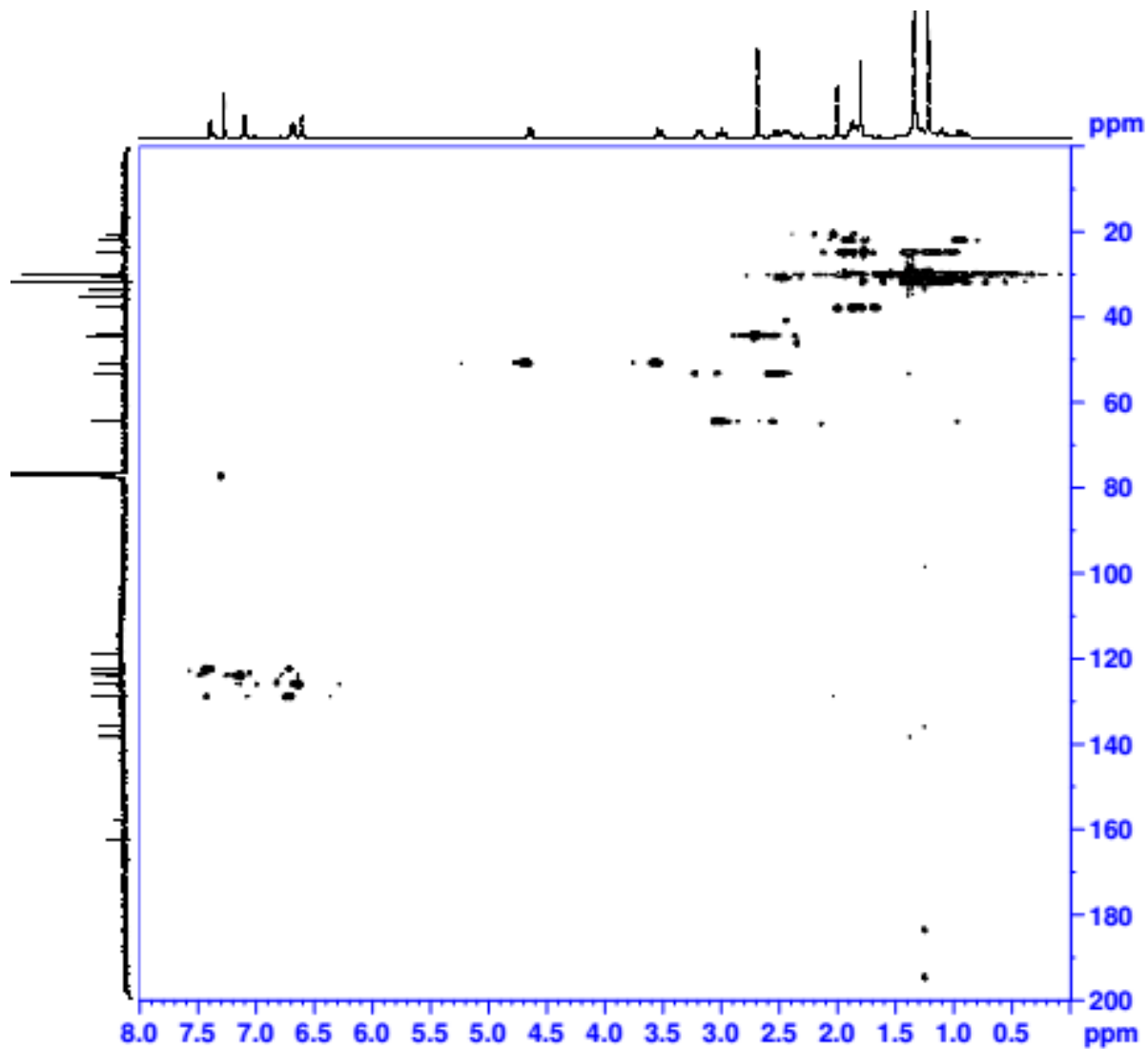


**Figure S7.**  $^1\text{H} - ^{13}\text{C}$  HMBC ( $\text{CDCl}_3$ , 25 °C) spectrum of  $(\pm)$ - $[ (\text{NNO})\text{InCl}]_2(\mu\text{-Cl})(\mu\text{-OPh}_{\text{Me}})$  (**2**)

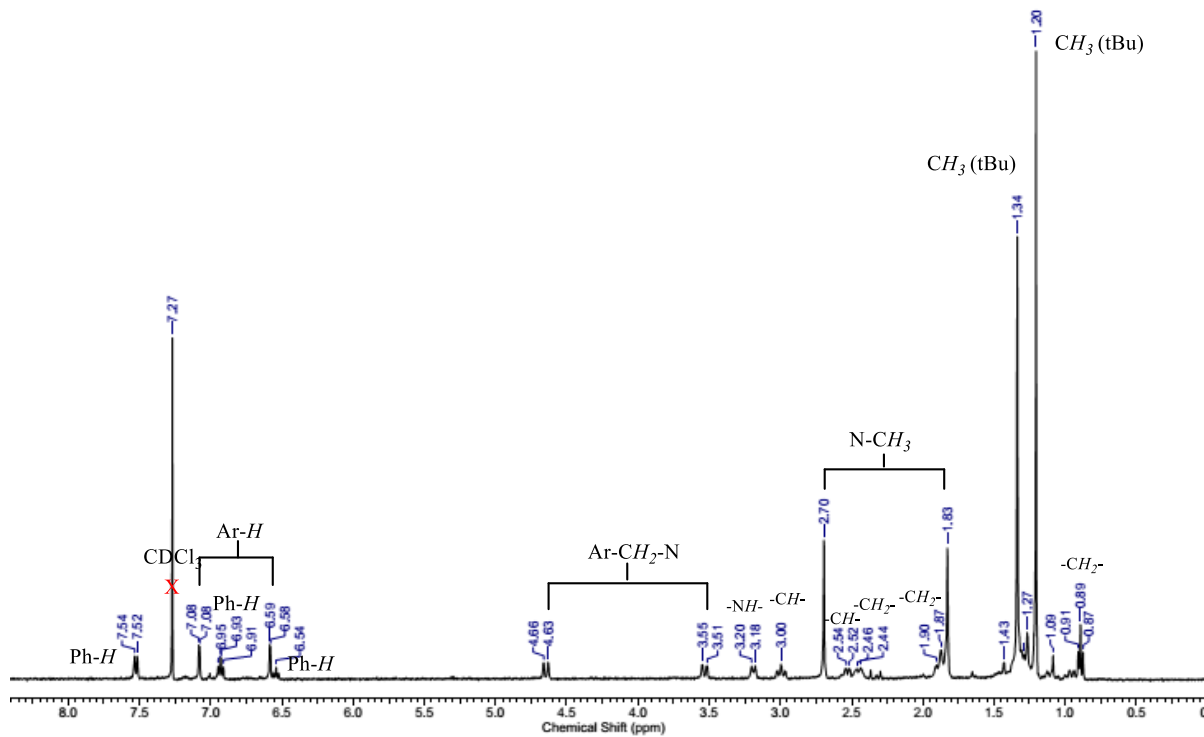


**Figure S8.**  $^1\text{H}$  NMR ( $\text{CDCl}_3$ , 25 °C) spectrum of  $(\pm)$ - $[ (\text{NNO})\text{InCl}]_2(\mu\text{-Cl})(\mu\text{-OPh}_\text{H})$  (**3**)

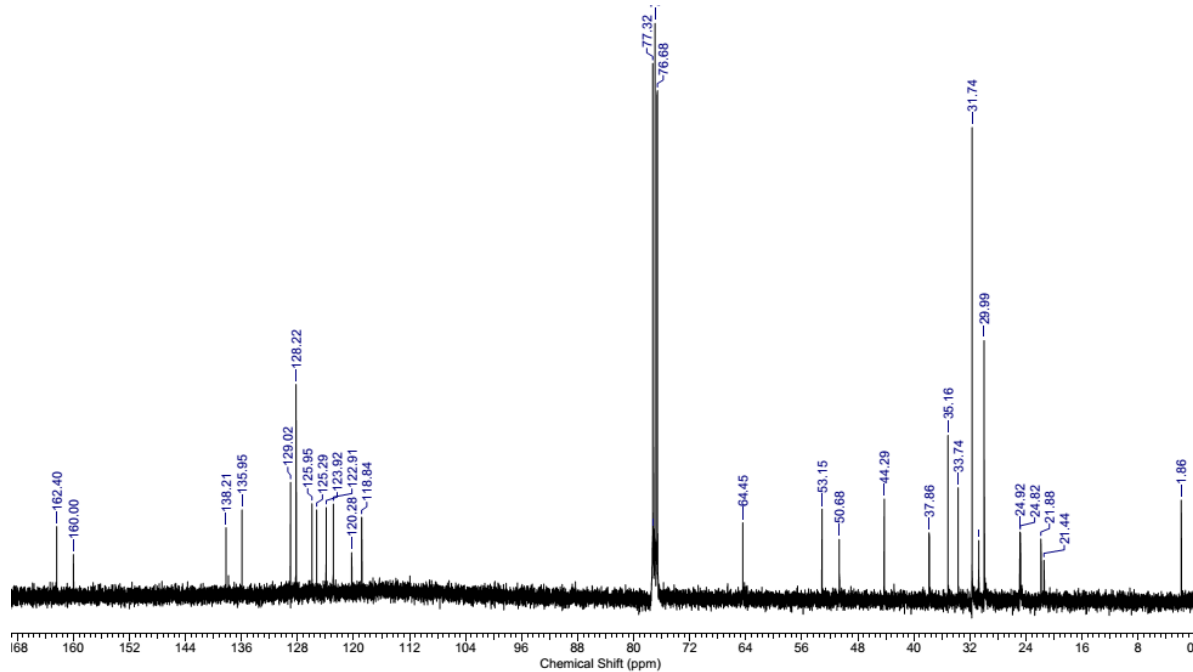


**Figure S9.**  $^{13}\text{C}\{\text{H}\}$  NMR ( $\text{CDCl}_3$ , 25 °C) spectrum  $(\pm)$ - $[ (\text{NNO})\text{InCl}]_2(\mu\text{-Cl})(\mu\text{-OPh}_\text{H})$  (**3**)

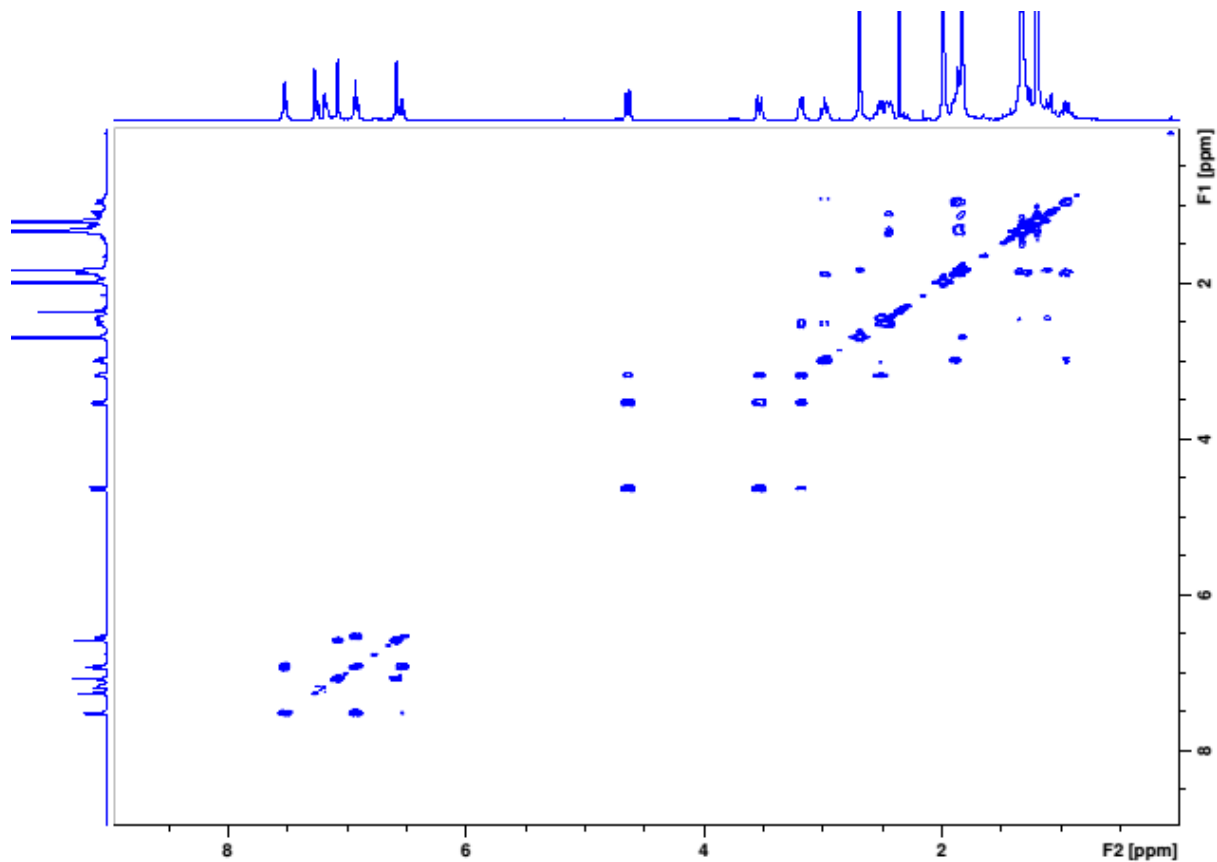


**Figure S10.** <sup>1</sup>H – <sup>1</sup>H COSY ( $\text{CDCl}_3$ , 25 °C) spectrum of  $(\pm)$ - $[(\text{NNO})\text{InCl}]_2(\mu\text{-Cl})(\mu\text{-OPh}_\text{H})$  (**3**)

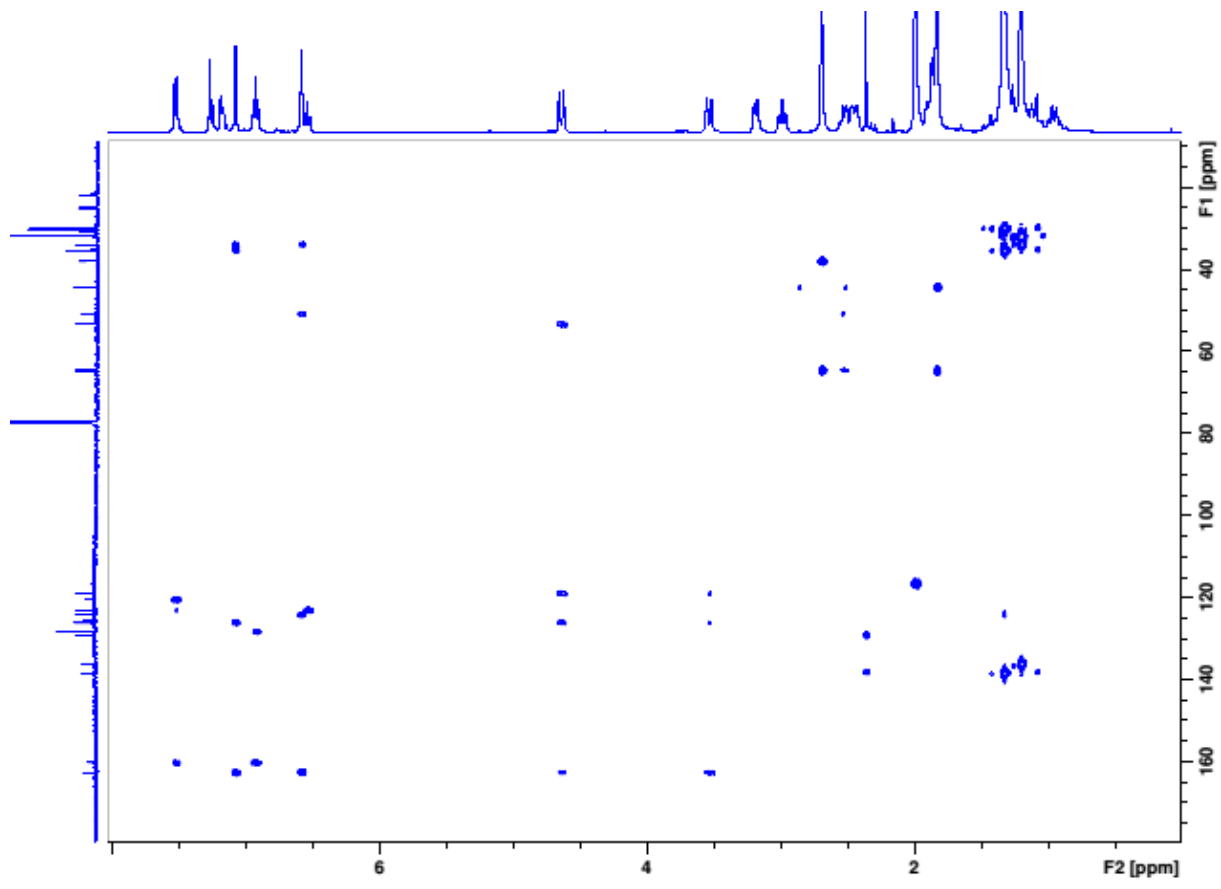


**Figure S11.** <sup>1</sup>H - <sup>13</sup>C HMBC ( $\text{CDCl}_3$ , 25 °C) spectrum ( $\pm$ )- $[(\text{NNO})\text{InCl}]_2(\mu\text{-Cl})(\mu\text{-OPh}_\text{H})$  (3)

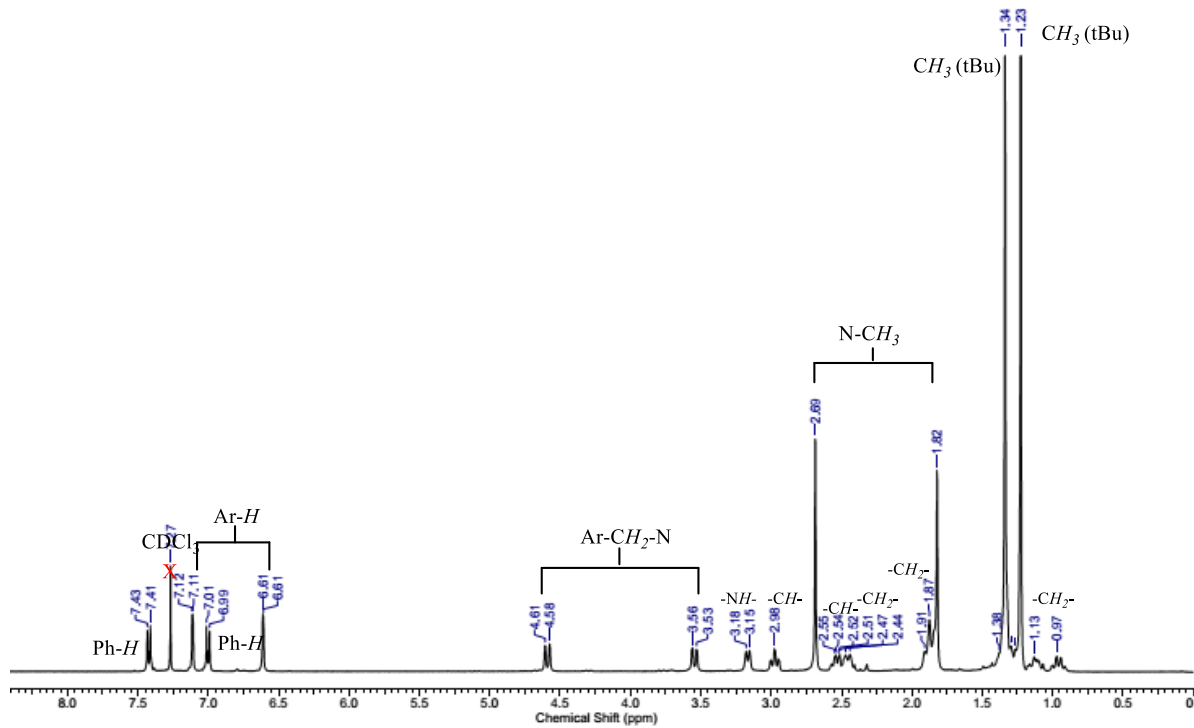


**Figure S12.**  $^1\text{H}$  NMR ( $\text{CDCl}_3$ , 25 °C) spectrum of  $(\pm)$ - $[ (\text{NNO})\text{InCl}]_2(\mu\text{-Cl})(\mu\text{-OPh}_{\text{Br}})$  (**4**)

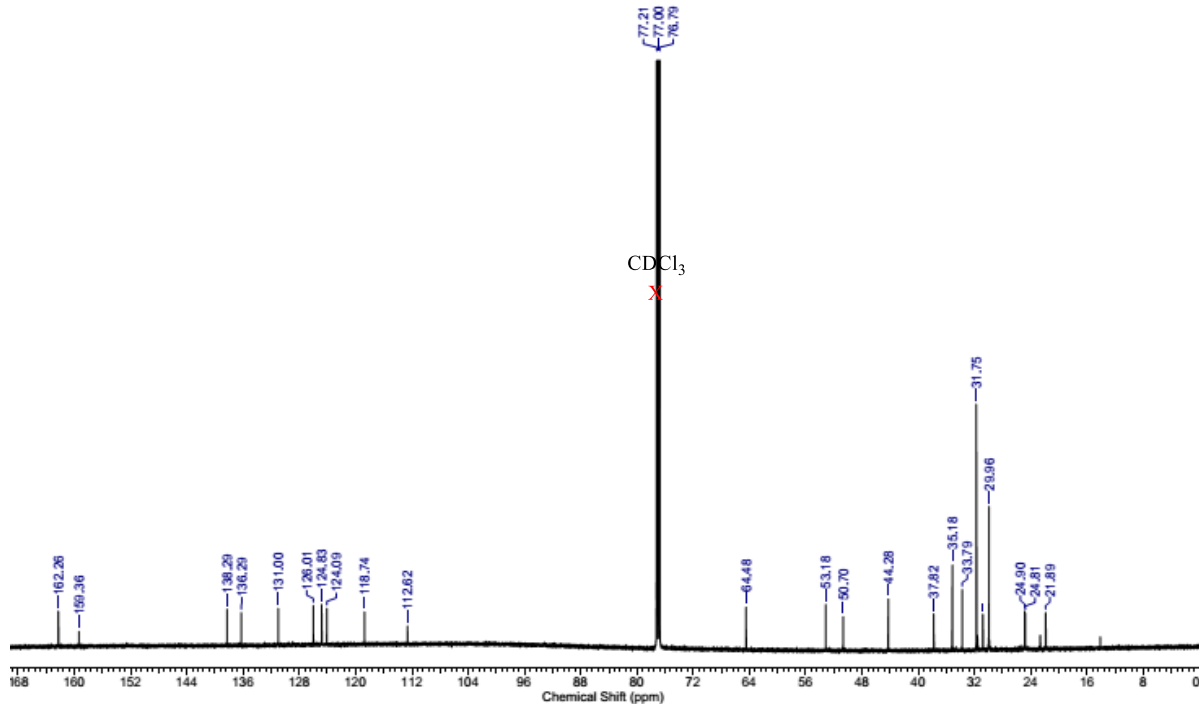


**Figure S13.**  $^{13}\text{C}\{^1\text{H}\}$  NMR ( $\text{CDCl}_3$ , 25 °C) spectrum of  $(\pm)$ - $[ (\text{NNO})\text{InCl}]_2(\mu\text{-Cl})(\mu\text{-OPh}_{\text{Br}})$  (**4**)

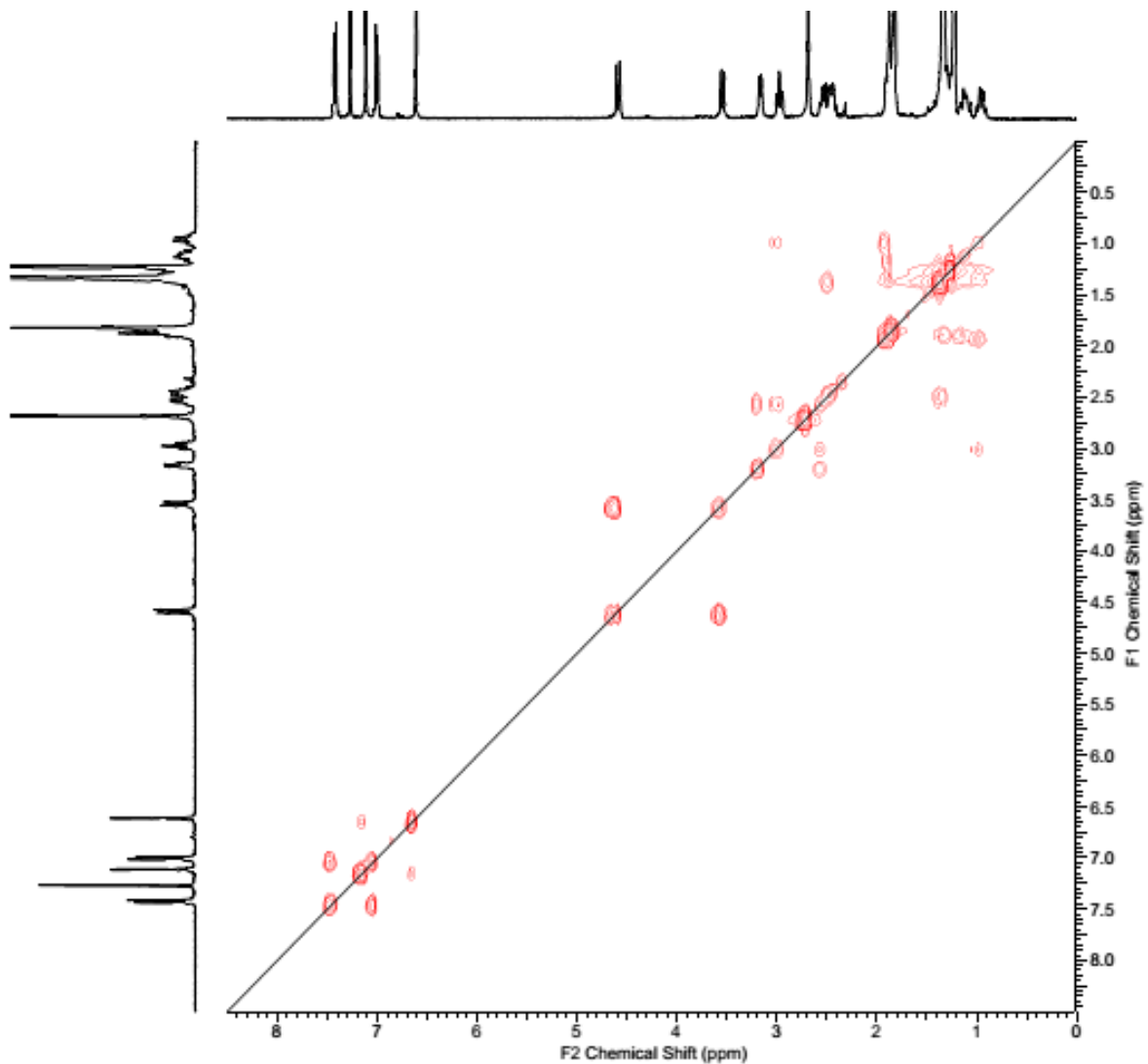


**Figure S14.** <sup>1</sup>H - <sup>1</sup>H COSY ( $\text{CDCl}_3$ , 25 °C) spectrum of  $(\pm)$ - $[ (\text{NNO})\text{InCl}]_2(\mu\text{-Cl})(\mu\text{-OPh}_{\text{Br}})$  (**4**)

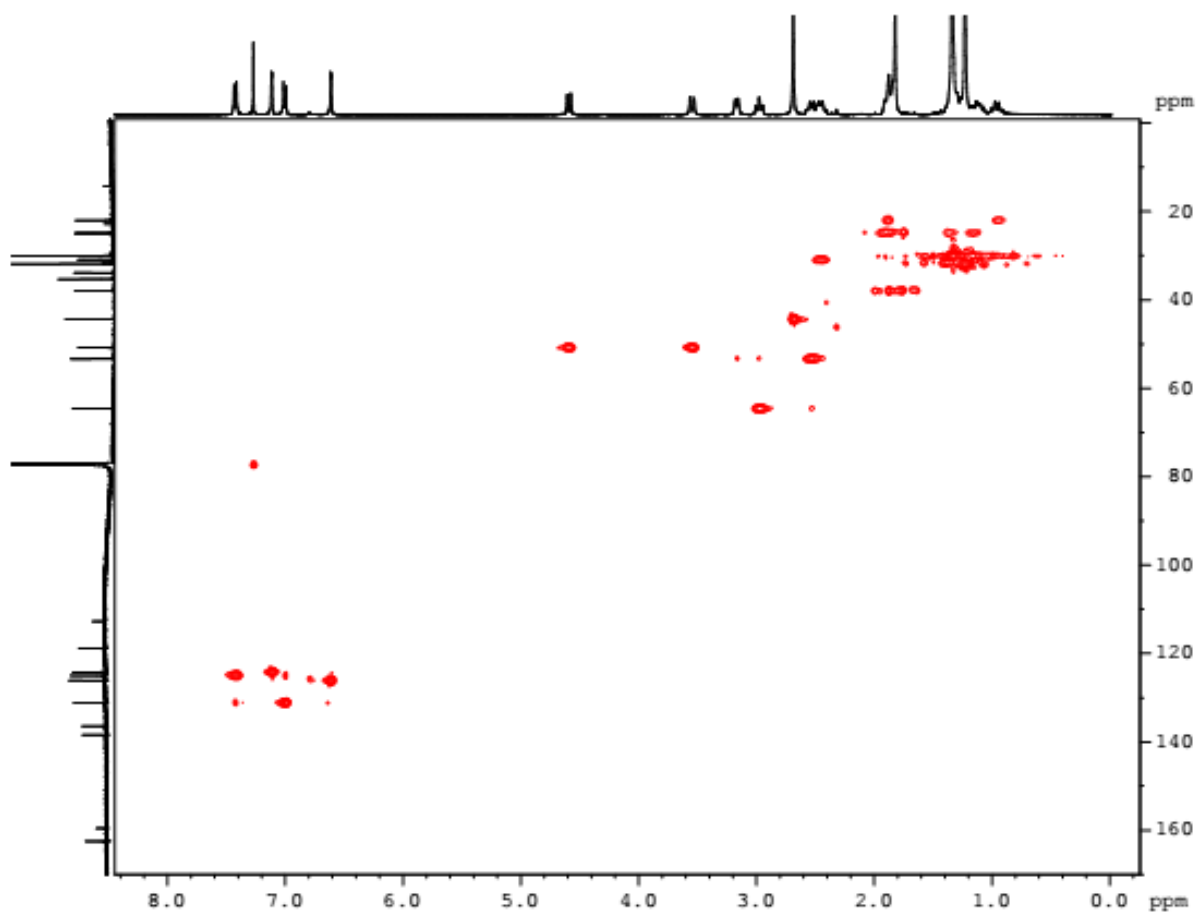


**Figure S15.**  $^1\text{H} - ^{13}\text{C}$  HMBC ( $\text{CDCl}_3$ , 25 °C) spectrum of  $(\pm)$ - $[(\text{NNO})\text{InCl}]_2(\mu\text{-Cl})(\mu\text{-OPh}_{\text{Br}})$  (**4**)

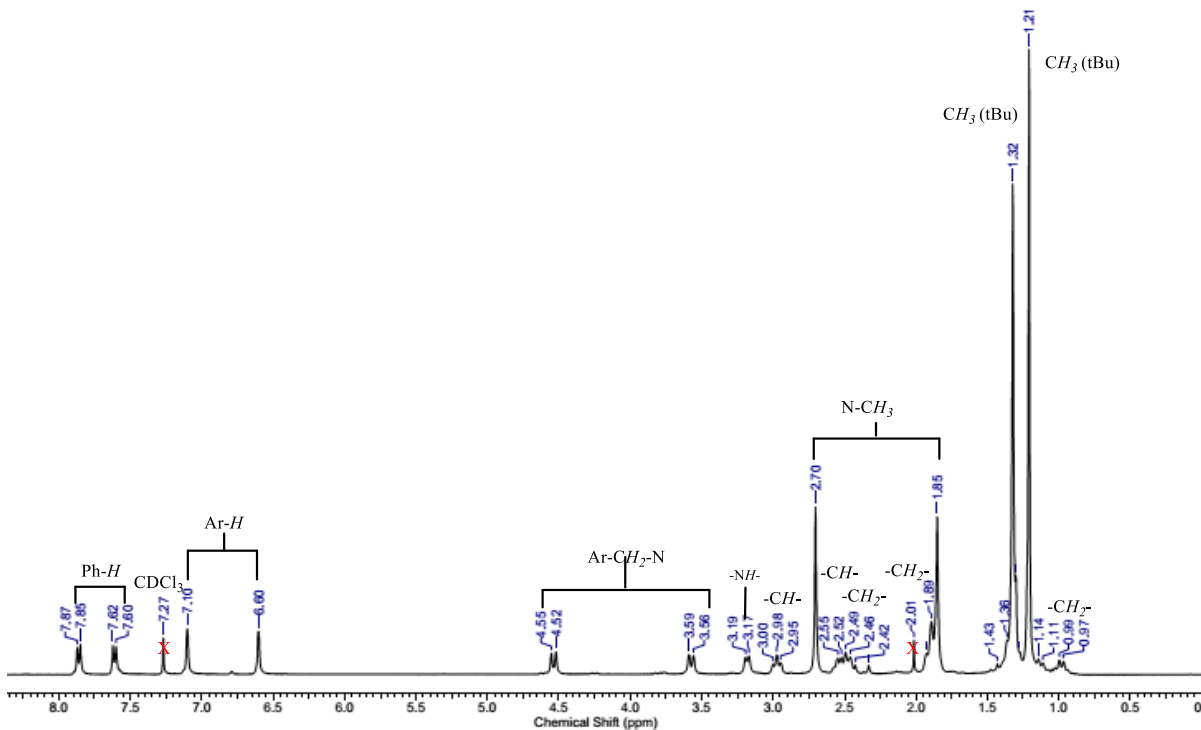


**Figure S16.**  $^1\text{H}$  NMR ( $\text{CDCl}_3$ , 25 °C) spectrum of  $(\pm)$ - $[ (\text{NNO})\text{InCl}]_2(\mu\text{-Cl})(\mu\text{-OPh}_{\text{NO}_2})$  (**5**)

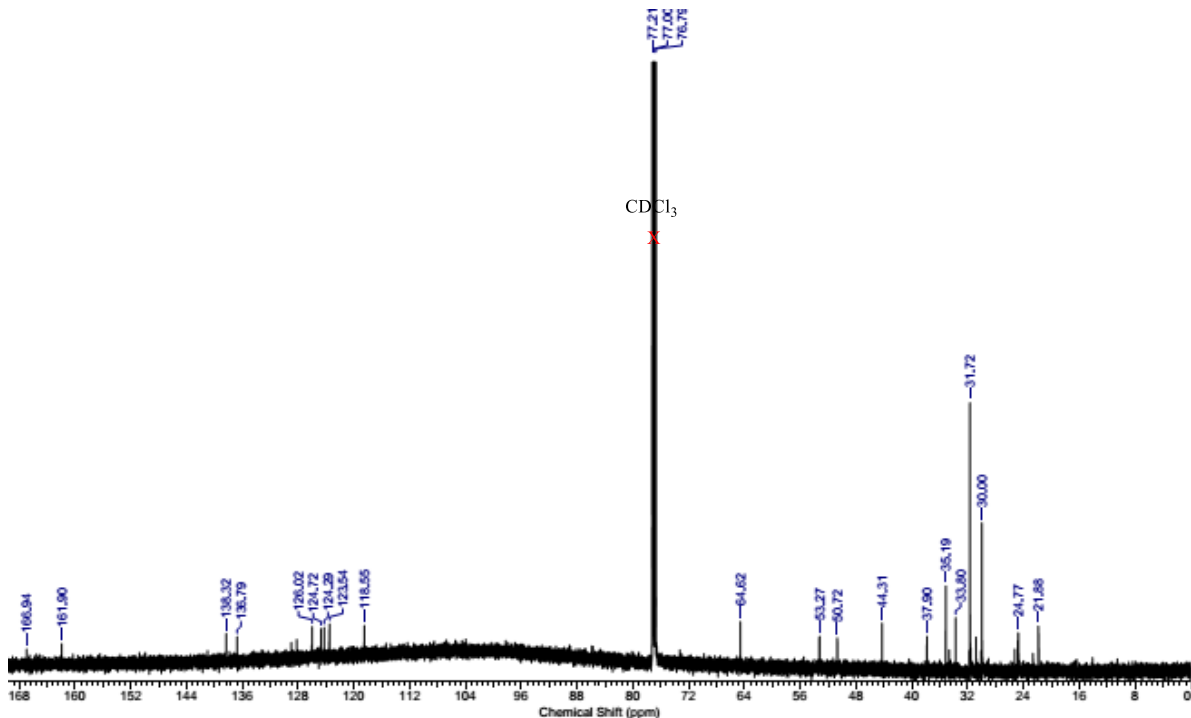


**Figure S17.**  $^{13}\text{C}\{^1\text{H}\}$  NMR ( $\text{CDCl}_3$ , 25 °C) spectrum of  $(\pm)$ - $[ (\text{NNO})\text{InCl}]_2(\mu\text{-Cl})(\mu\text{-OPh}_{\text{NO}_2})$  (**5**)

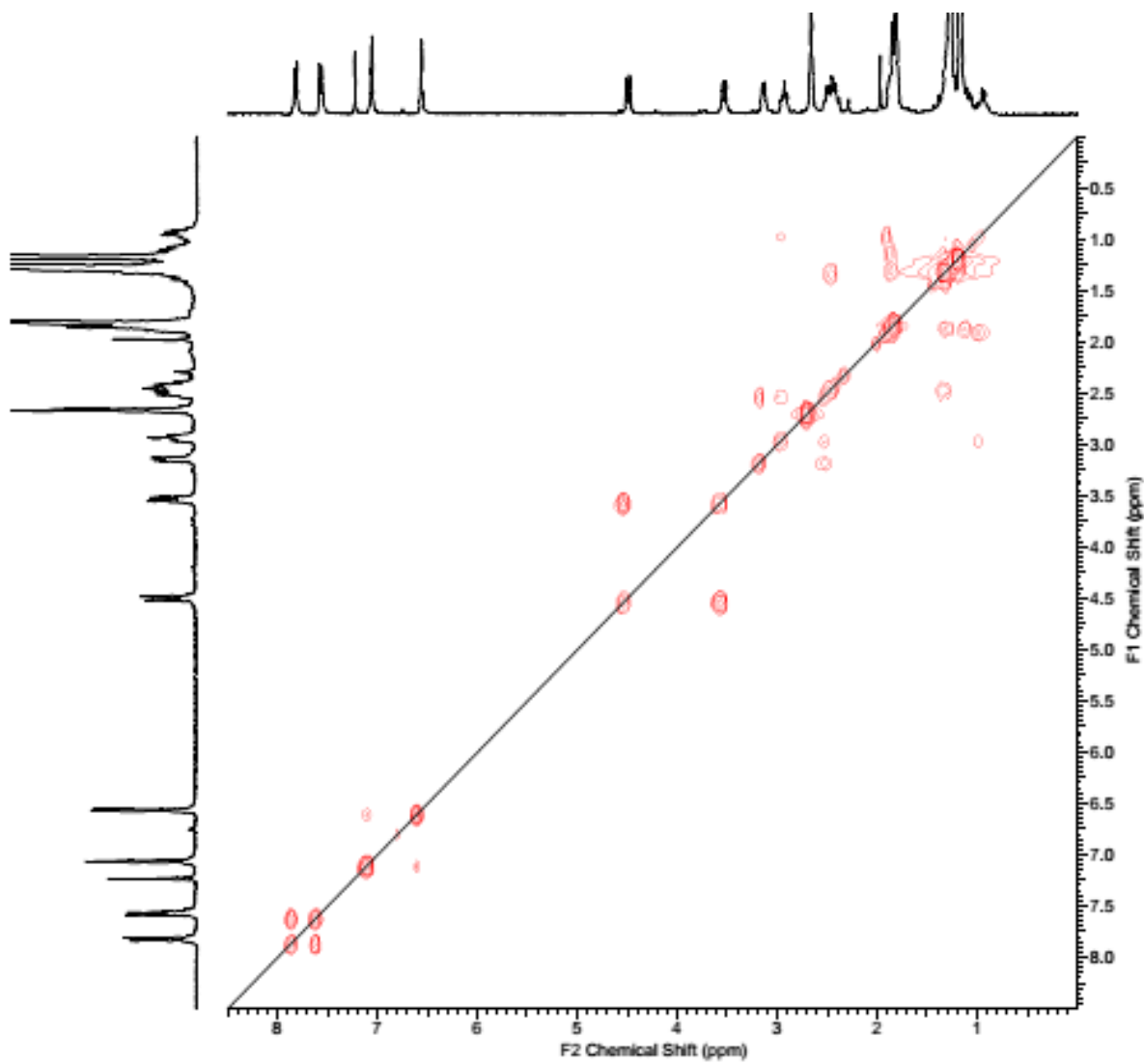


**Figure S18.**  $^1\text{H}$  –  $^1\text{H}$  COSY ( $\text{CDCl}_3$ , 25 °C) spectrum of  $(\pm)$ - $[(\text{NNO})\text{InCl}]_2(\mu\text{-Cl})(\mu\text{-OPh}_{\text{NO}_2})$  (**5**)

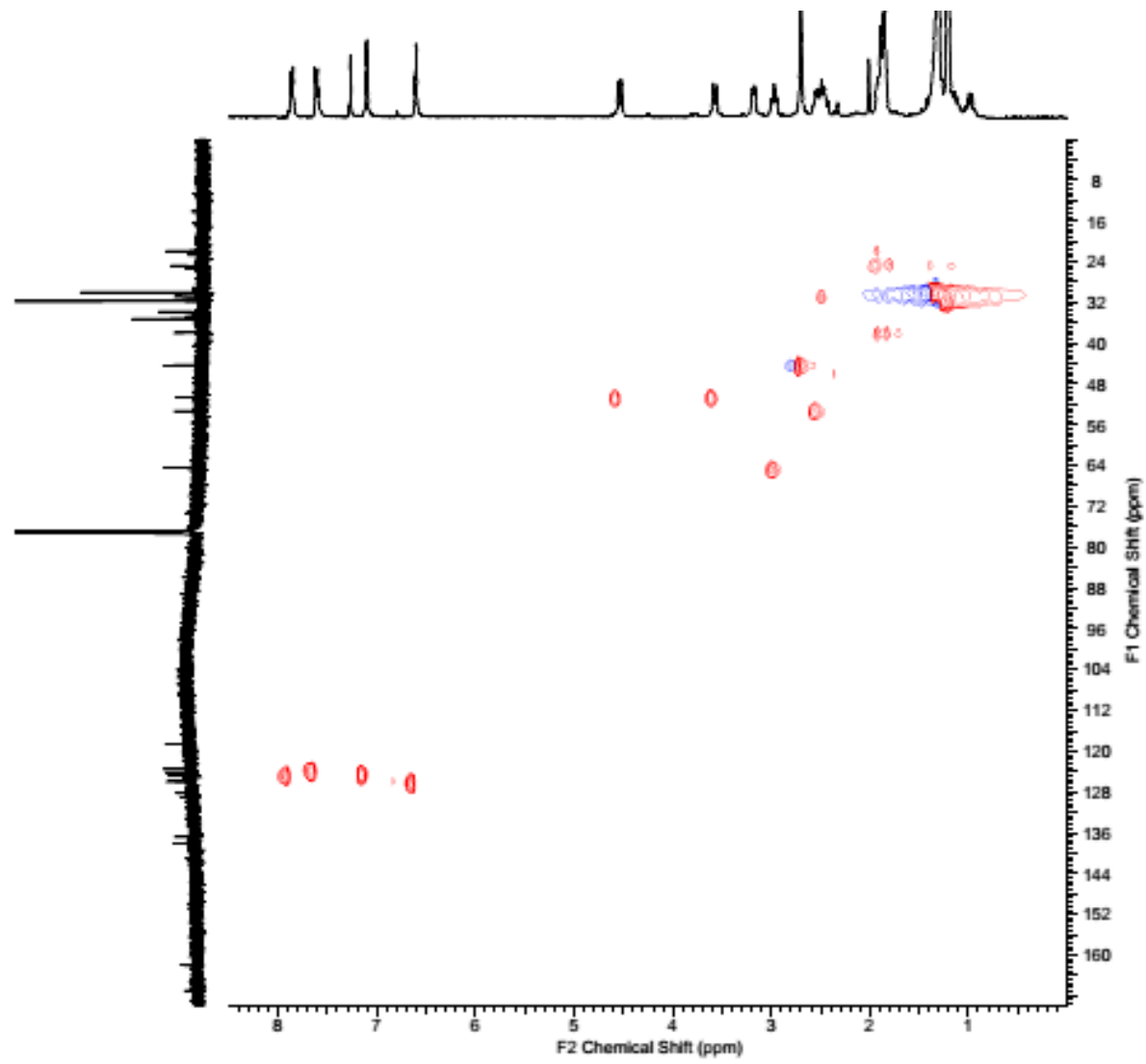


**Figure S19.**  $^1\text{H} - ^{13}\text{C}$  HMBC ( $\text{CDCl}_3$ , 25 °C) spectrum of  $(\pm)$ - $[(\text{NNO})\text{InCl}]_2(\mu\text{-Cl})(\mu\text{-OPh}_{\text{NO}_2})$  (**5**)

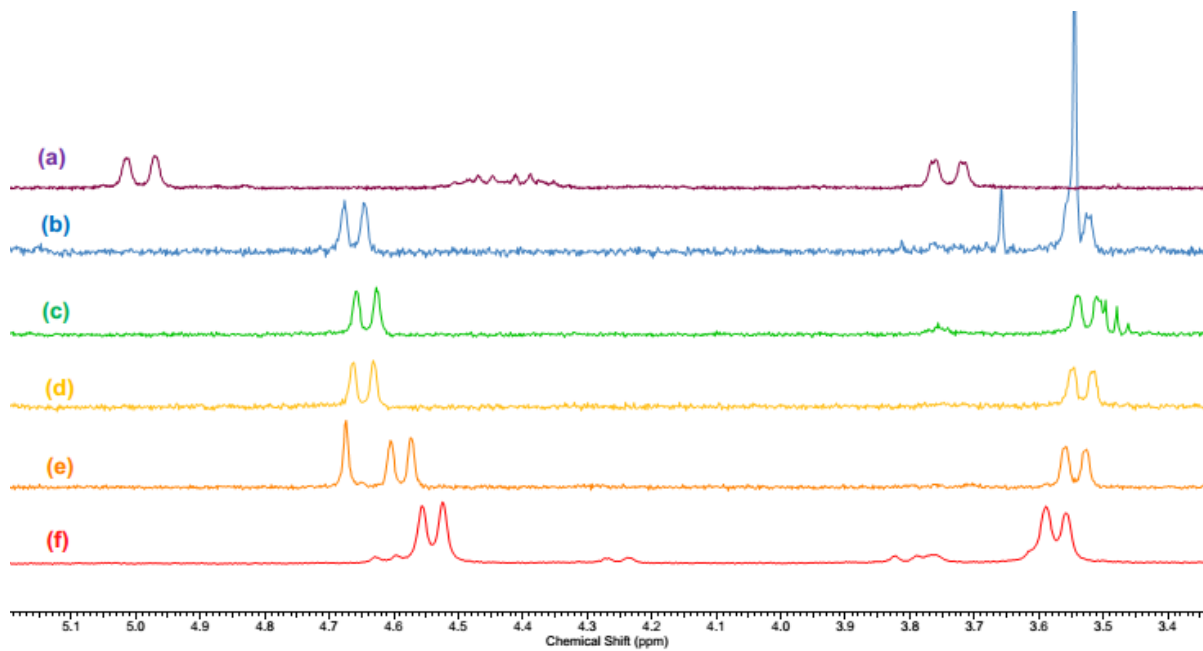


**Figure S20.**  $^1\text{H}$  NMR spectra ( $\text{CDCl}_3$ , 25 °C) diastereotopic ligand  $\text{NH}-\text{CH}_2-\text{Ar}$  protons for (a)  $[(\text{NNO})\text{InCl}]_2(\mu\text{-Cl})(\mu\text{-OEt})$  (**A**), (b)  $[(\text{NNO})\text{InCl}]_2(\mu\text{-Cl})(\mu\text{-OPh}_{\text{OMe}})$  (**1**), (c)  $[(\text{NNO})\text{InCl}]_2(\mu\text{-Cl})(\mu\text{-OPh}_{\text{Me}})$  (**2**), (d)  $[(\text{NNO})\text{InCl}]_2(\mu\text{-Cl})(\mu\text{-OPh}_{\text{H}})$  (**3**), (e)  $[(\text{NNO})\text{InCl}]_2(\mu\text{-Cl})(\mu\text{-OPh}_{\text{Br}})$  (**4**), and (f)  $[(\text{NNO})\text{InCl}]_2(\mu\text{-Cl})(\mu\text{-OPh}_{\text{NO}_2})$  (**5**)

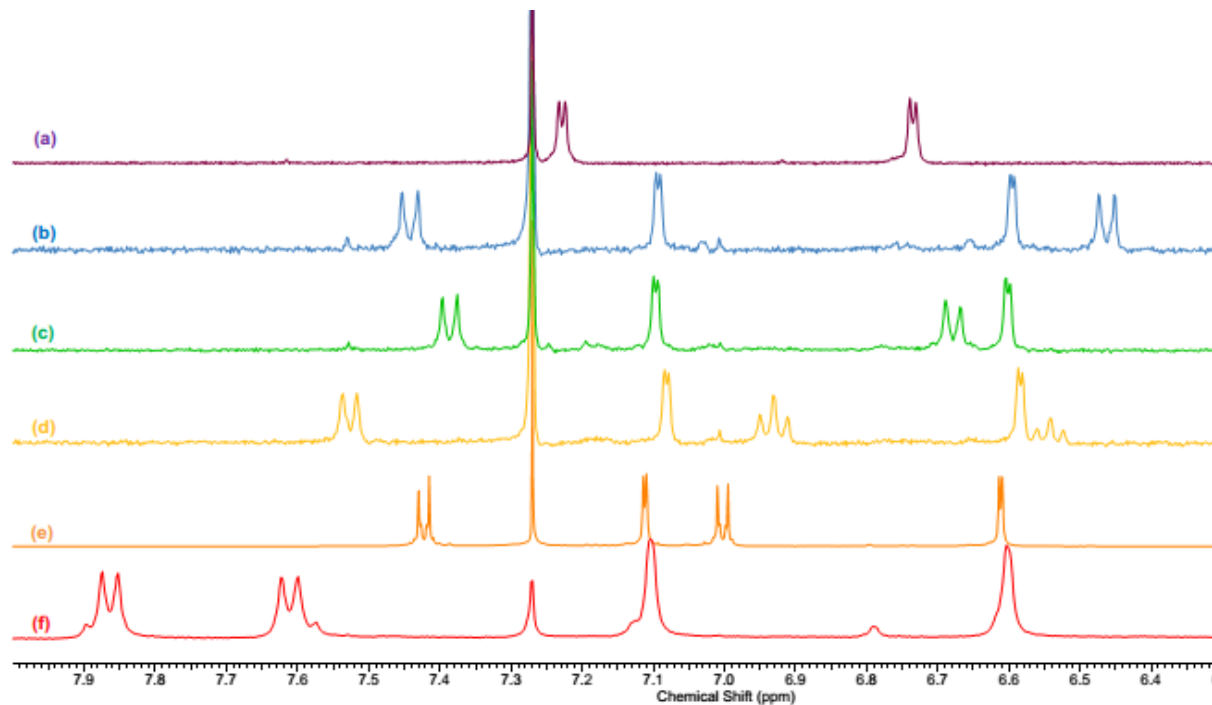


**Figure S21.**  $^1\text{H}$  NMR spectra ( $\text{CDCl}_3$ , 25 °C) bridging phenolic protons for (a)  $[(\text{NNO})\text{InCl}]_2(\mu\text{-Cl})(\mu\text{-OEt})$  (**A**), (b)  $[(\text{NNO})\text{InCl}]_2(\mu\text{-Cl})(\mu\text{-OPh}_{\text{OMe}})$  (**1**), (c)  $[(\text{NNO})\text{InCl}]_2(\mu\text{-Cl})(\mu\text{-OPh}_{\text{Me}})$  (**2**), (d)  $[(\text{NNO})\text{InCl}]_2(\mu\text{-Cl})(\mu\text{-OPh}_{\text{H}})$  (**3**), (e)  $[(\text{NNO})\text{InCl}]_2(\mu\text{-Cl})(\mu\text{-OPh}_{\text{Br}})$  (**4**), and (f)  $[(\text{NNO})\text{InCl}]_2(\mu\text{-Cl})(\mu\text{-OPh}_{\text{NO}_2})$  (**5**)

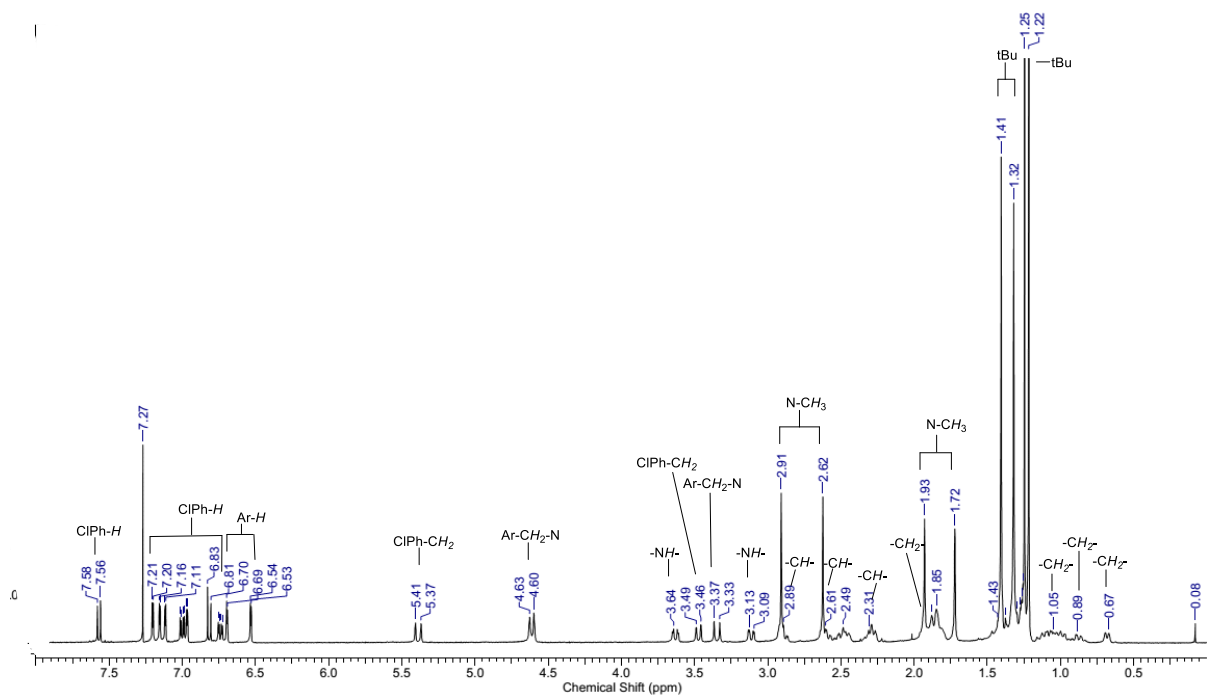


**Figure S22.**  $^1\text{H}$  NMR ( $\text{CDCl}_3$ , 25 °C) spectrum of  $(\pm)$ - $[ (\text{NNO})\text{InCl}]_2(\mu\text{-Cl})(\kappa^2,\mu\text{-diClPh})$  (**6**)

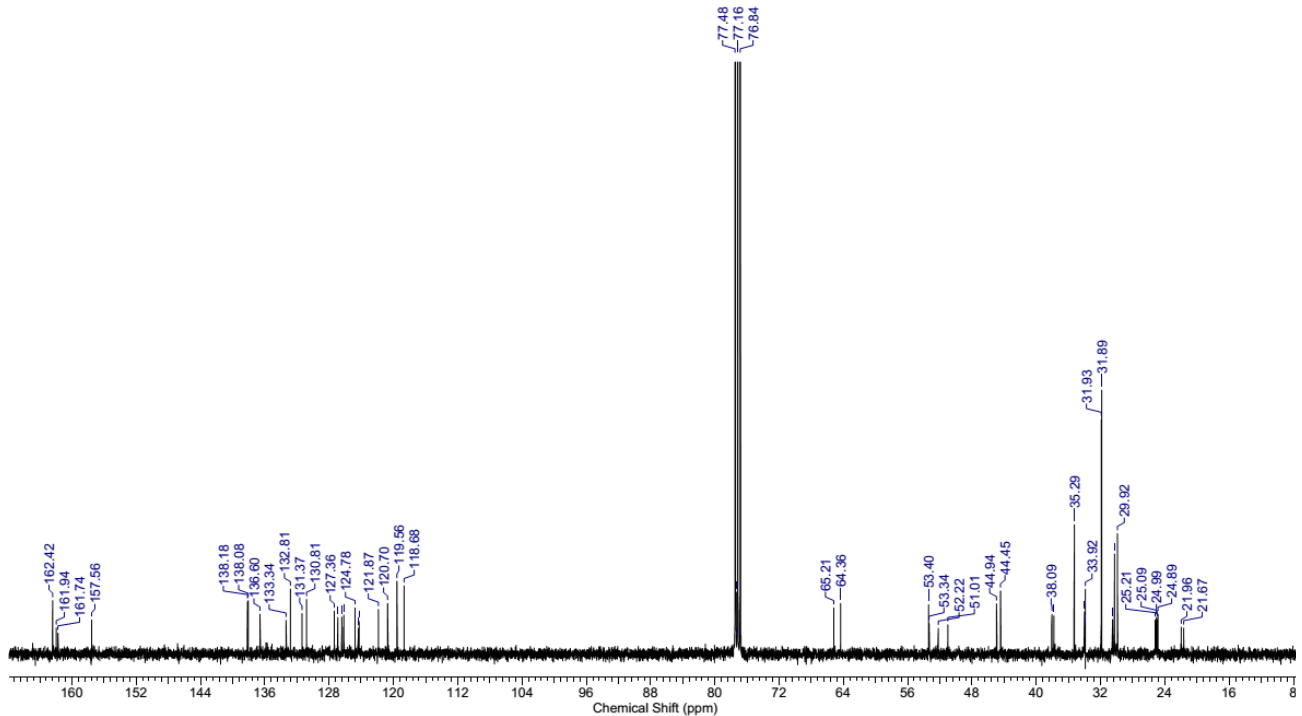


**Figure S23.**  $^{13}\text{C}\{^1\text{H}\}$  NMR ( $\text{CDCl}_3$ , 25 °C) spectrum of  $(\pm)$ - $[ (\text{NNO})\text{InCl}]_2(\mu\text{-Cl})(\kappa^2,\mu\text{-diClPh})$  (**6**)

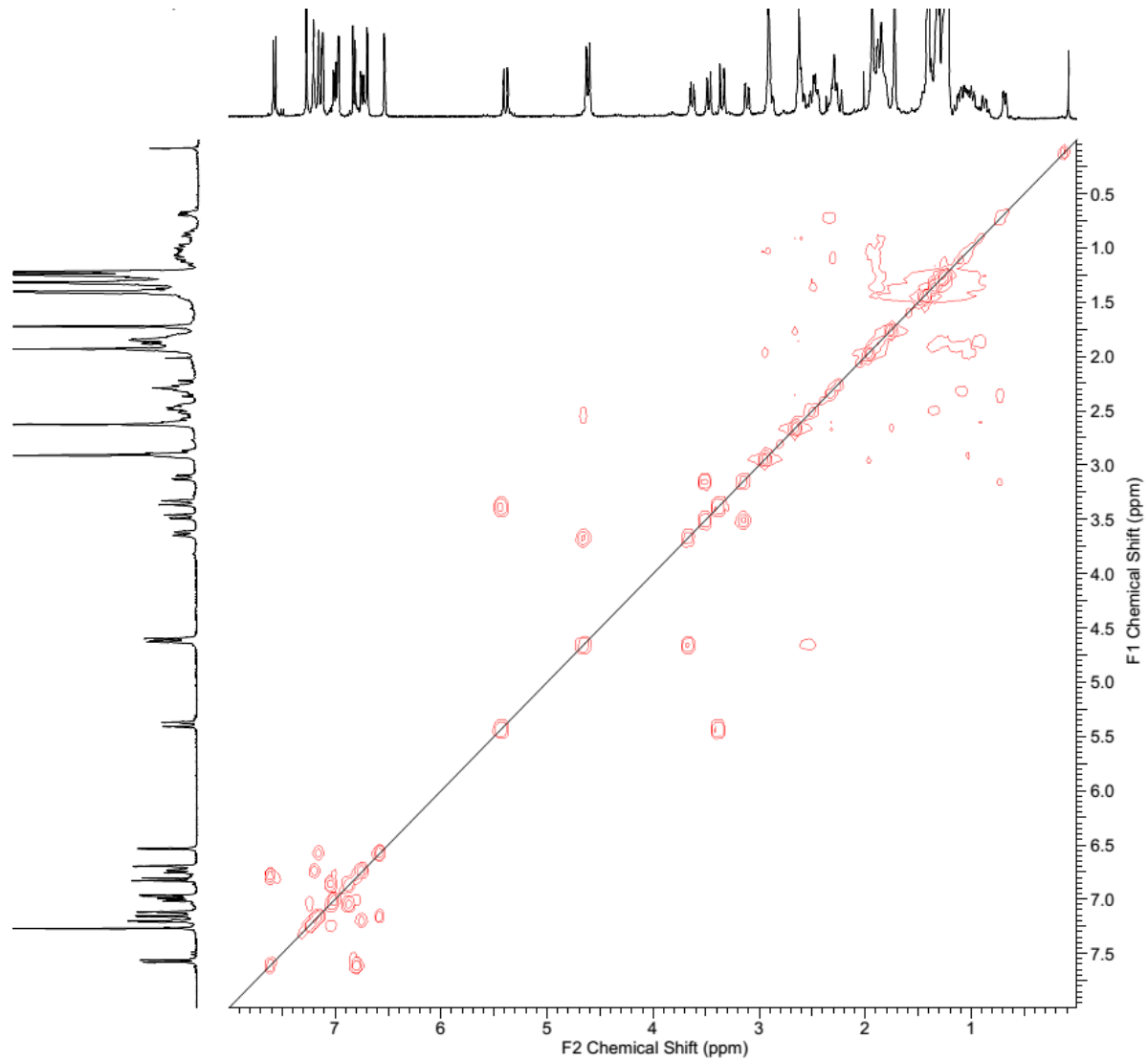


**Figure S24.**  $^1\text{H}$  -  $^1\text{H}$  COSY ( $\text{CDCl}_3$ ,  $25^\circ\text{C}$ ) spectrum of  $(\pm)$ - $[(\text{NNO})\text{InCl}]_2(\mu\text{-Cl})(\kappa^2,\mu\text{-diClPh})$  (6)

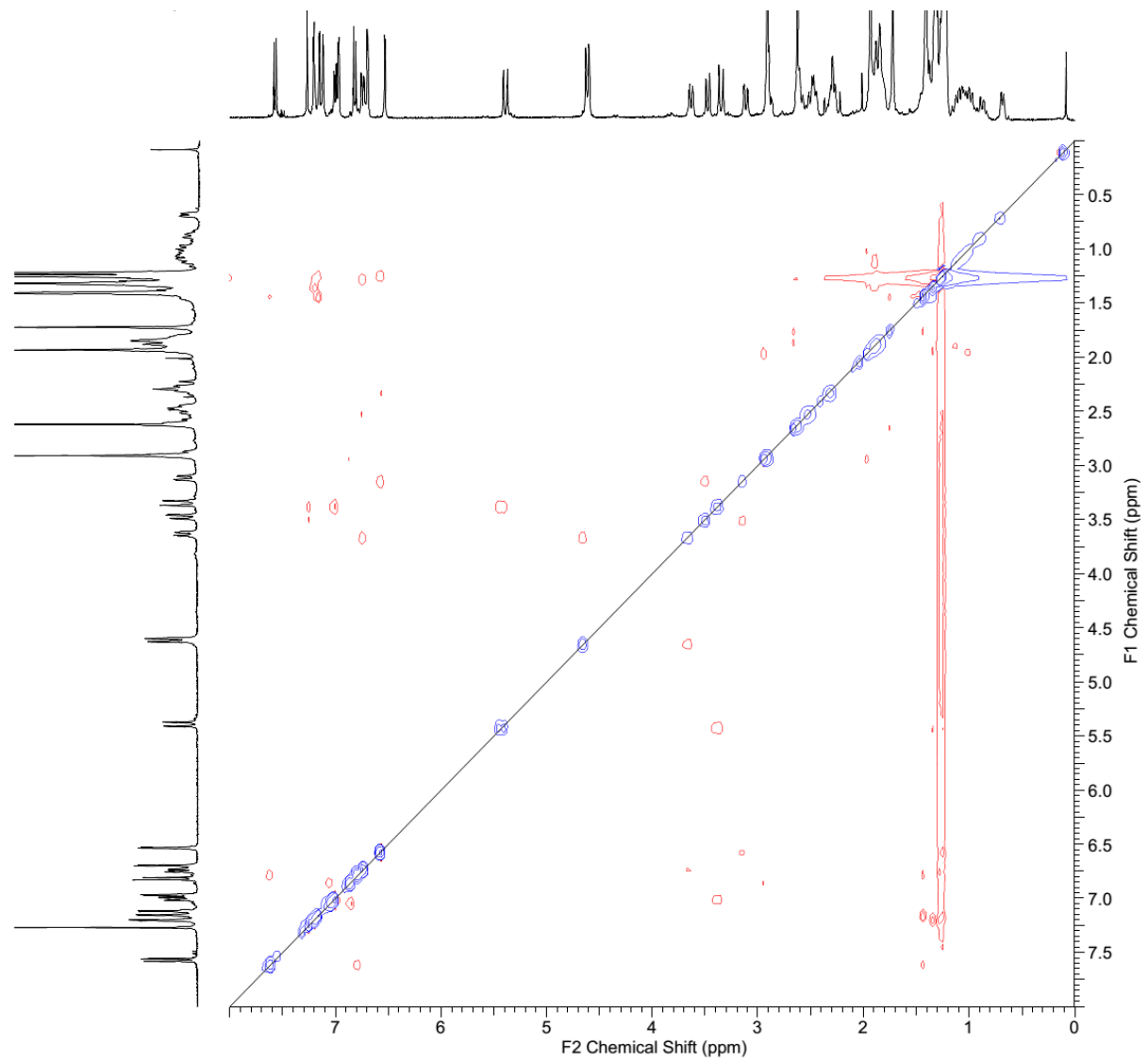


**Figure S25.**  $^1\text{H} - ^1\text{H}$  NOESY ( $\text{CDCl}_3$ , 25 °C) spectrum of  $(\pm)$ - $[ (\text{NNO})\text{InCl}]_2(\mu\text{-Cl})(\kappa^2,\mu\text{-diClPh})$  (6)

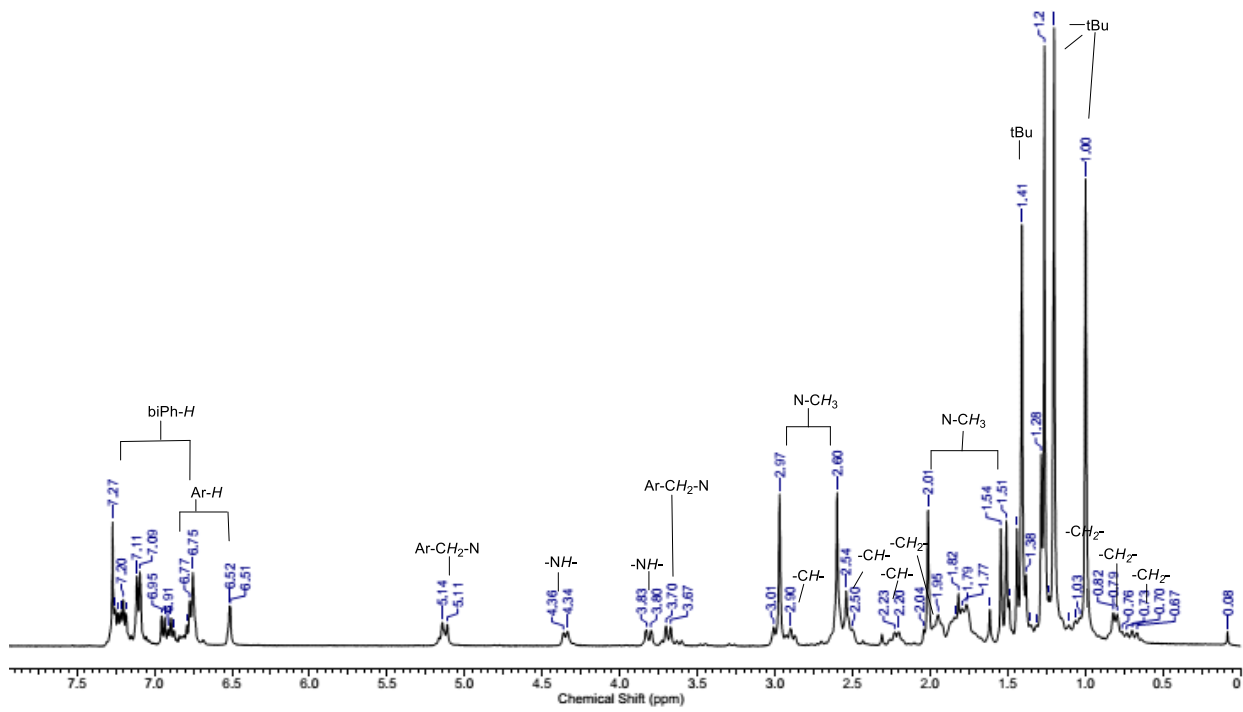


**Figure S26.**  $^1\text{H}$  ( $\text{CDCl}_3$ , 25 °C) spectrum of  $(\pm)$ - $[ (\text{NNO})\text{InCl}]_2(\mu\text{-Cl})(\kappa^2,\mu\text{-biPh})$ .

## B. Characterization of complexes 2-6 in the solid state

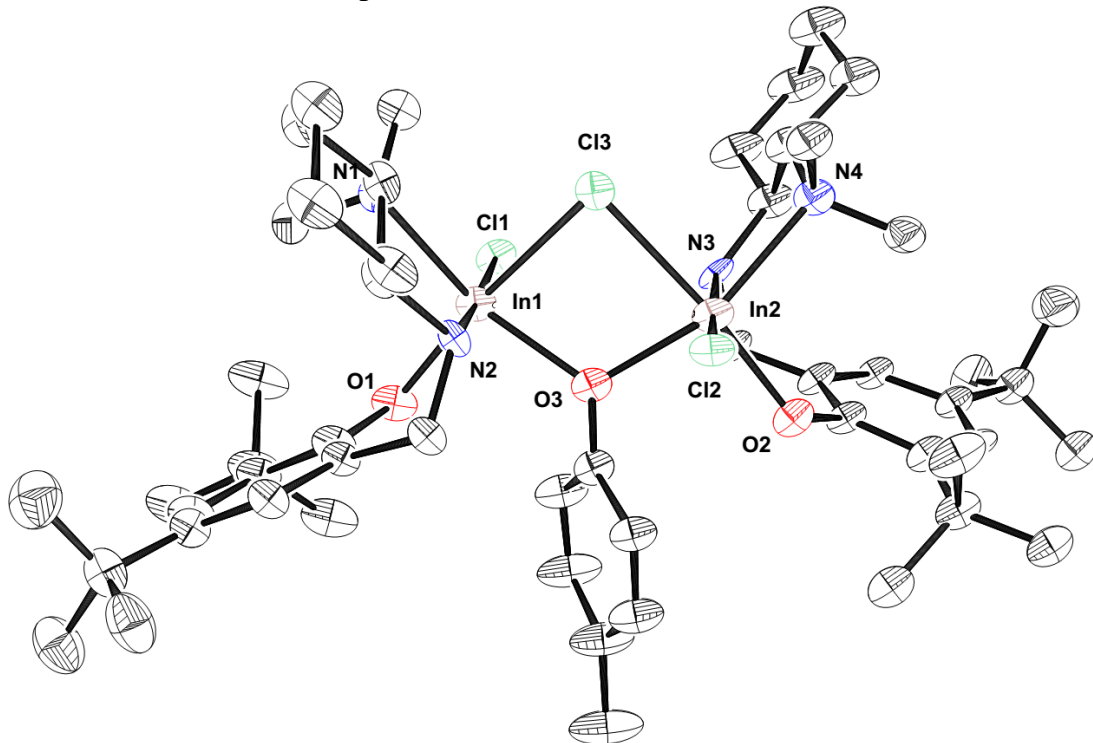


**Figure S27.** Molecular structure of  $[(\text{NNO})\text{InCl}]_2(\mu\text{-Cl})(\mu\text{-OPh}_\text{Me})$  (**2**) depicted with ellipsoids at 50% probability (H atoms and all solvent molecules omitted for clarity). Selected bond lengths (Å): In1-Cl1 2.423(3), In1-Cl3 2.615(4), In1-O1 2.081(10), In1-O3 2.198(11), In1-N1 2.358(14), In1-N2 2.276(10), In2-Cl2 2.423(3), In2-Cl3 2.627(4), In2-O2 2.066(11), In2-O3 2.174(11), In2-N3 2.345(12), In2-N4 2.270(10). Selected bond angles (deg): O3-In1-Cl3 78.5(3), O3-In1-Cl1 94.2(2), O3-In1-N1 158.7(4), O3-In1-N2 89.1(4), O1-In1-Cl3 171.7(3).

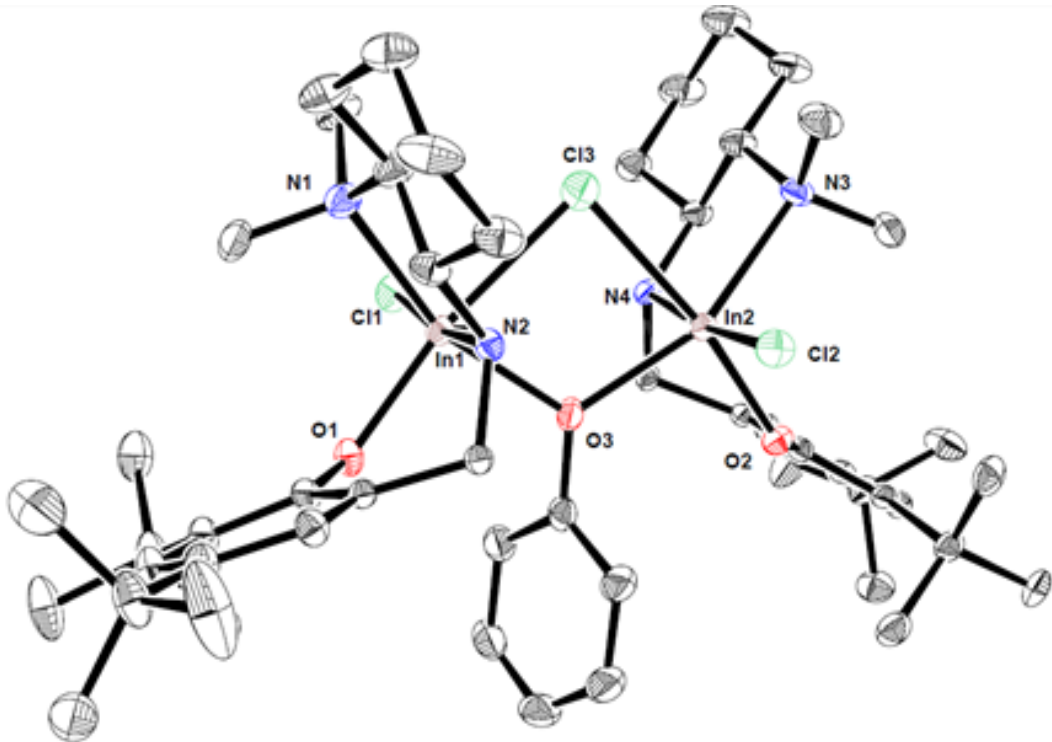


**Figure S28.** Molecular structure of  $[(\text{NNO})\text{InCl}]_2(\mu\text{-Cl})(\mu\text{-OPhH})$  (**3**) depicted with ellipsoids at 50% probability (H atoms and all solvent molecules omitted for clarity). Selected bond lengths (Å): In1-Cl1 2.4261(8), In1-Cl3 2.6019(9), In1-O1 2.072(2), In1-O3 2.186(2), In1-N1 2.352(3), In1-N2 2.259(2), In2-Cl2 2.4239(8), In2-Cl3 2.6451(9), In2-O2 2.082(2), In2-O3 2.174(2), In2-N3 2.337(3), In2-N4 2.250(2). Selected bond angles (deg): O3-In1-Cl3 78.80(6), O3-In1-Cl1 95.56(6), O3-In1-N1 157.84(9), O3-In1-N2 88.79(8), O1-In1-Cl3 170.58(6).

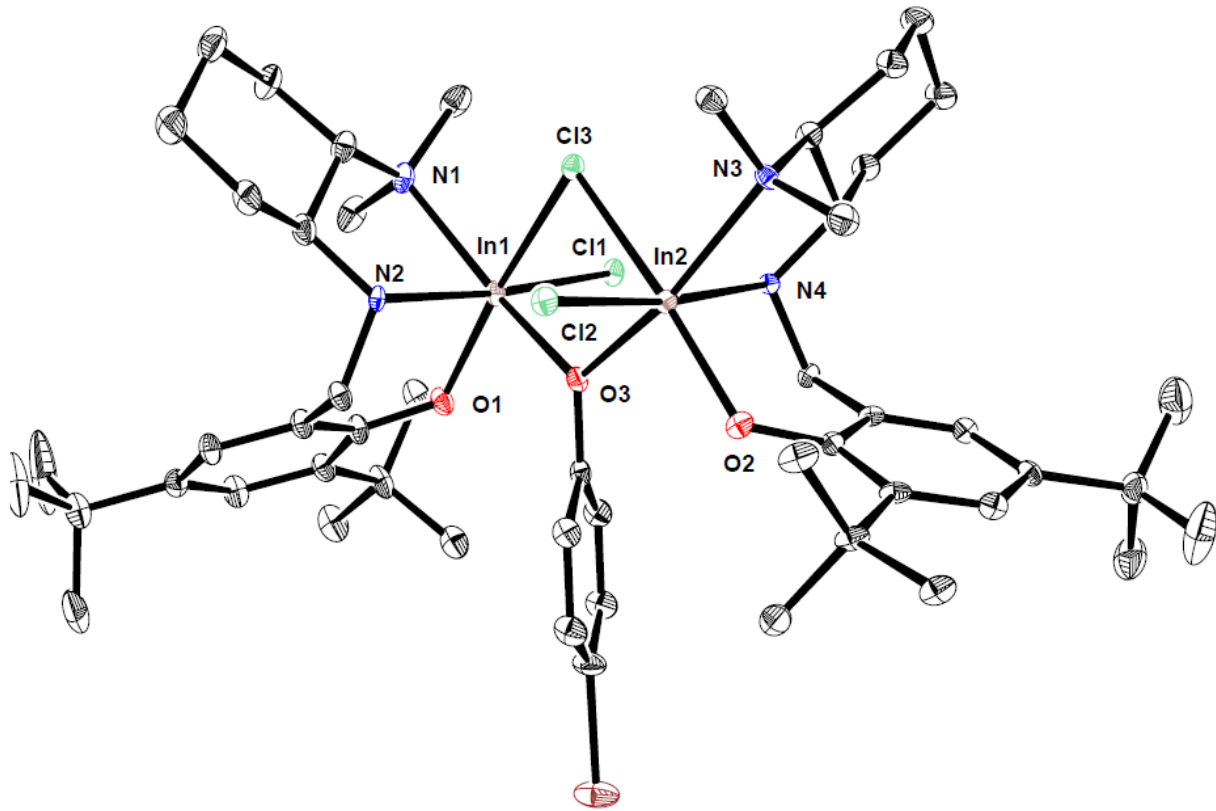


**Figure S29.** Molecular structure of  $[(\text{NNO})\text{InCl}]_2(\mu\text{-Cl})(\mu\text{-OPh}_{\text{Br}})$  (**4**) depicted with ellipsoids at 50% probability (H atoms and all solvent molecules omitted for clarity). Selected bond lengths (Å): In1-Cl1 2.4250(12), In1-Cl3 2.6202(13), In1-O1 2.063(4), In1-O3 2.191(3), In1-N1 2.318(5), In1-N2 2.262(4), In2-Cl2 2.4163(12), In2-Cl3 2.6296(13), In2-O2 2.063(3), In2-O3 2.186(3), In2-N3 2.335(4), In2-N4 2.257(5). Selected bond angles (deg): O3-In1-Cl3 77.89(9), O3-In1-Cl1 95.28(9), O3-In1-N1 158.24(14), O3-In1-N2 87.83(13), O1-In1-Cl3 170.70(11).

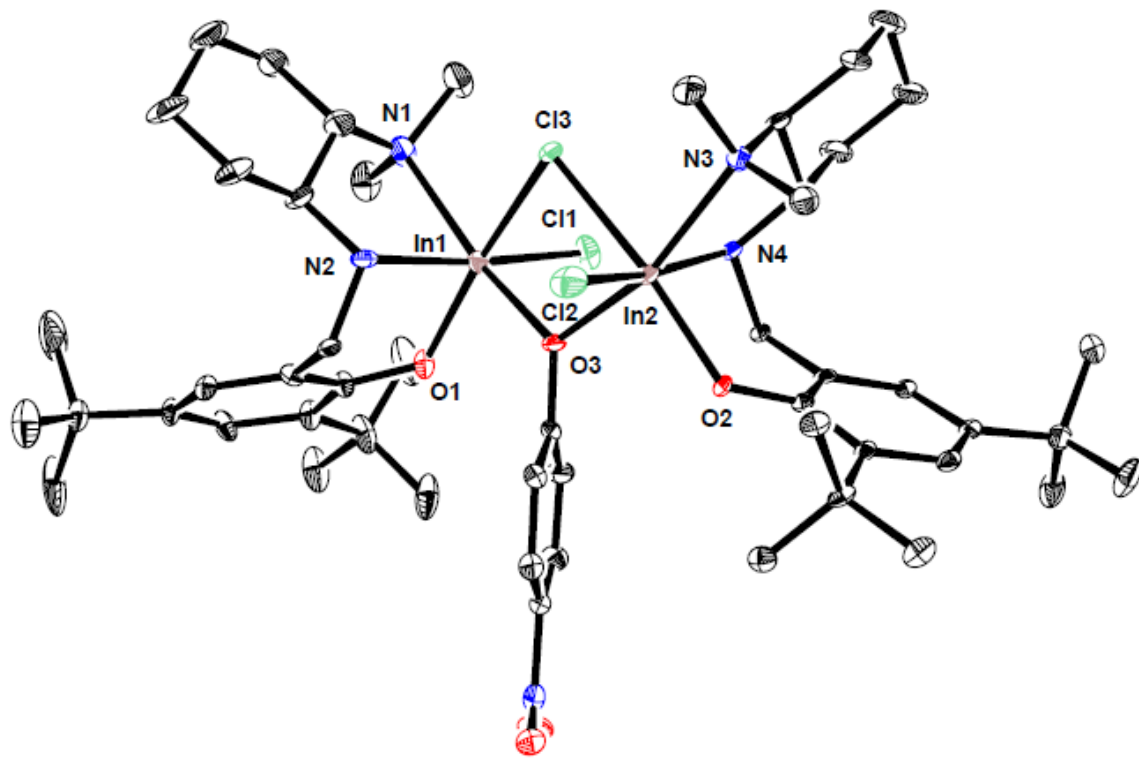


**Figure S30.** Molecular structure of  $[(\text{NNO})\text{InCl}]_2(\mu\text{-Cl})(\mu\text{-OPh}_{\text{NO}_2})$  (**5**) depicted with ellipsoids at 50% probability (H atoms and all solvent molecules omitted for clarity). Selected bond lengths ( $\text{\AA}$ ): In1-Cl1 2.4184(14), In1-Cl3 2.6126(14), In1-O1 2.065(4), In1-O3 2.193(4), In1-N1 2.316(4), In1-N2 2.251(4), In2-Cl2 2.4146(14), In2-Cl3 2.6250(14), In2-O2 2.067(3), In2-O3 2.203(4), In2-N3 2.328(4), In2-N4 2.255(4). Selected bond angles (deg): O3-In1-Cl3 77.13(10), O3-In1-Cl1 94.22(10), O3-In1-N1 158.80(15), O3-In1-N2 90.06(15), O1-In1-Cl3 167.69(11).

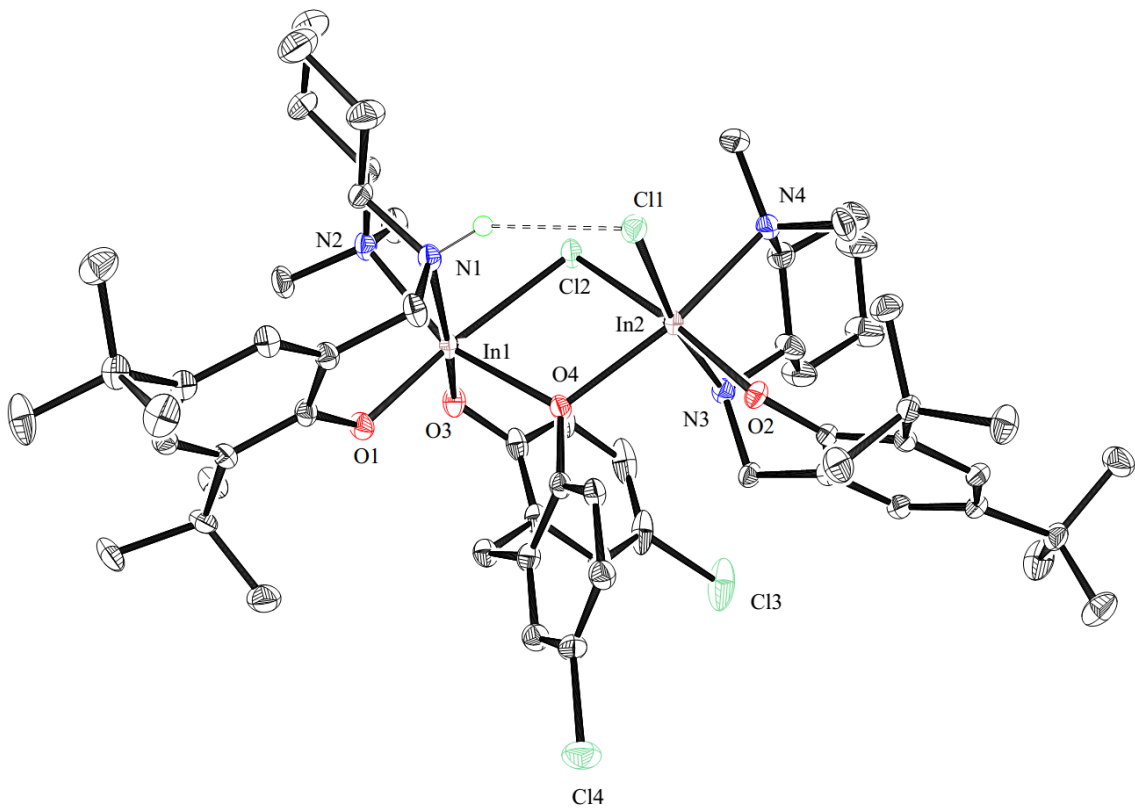
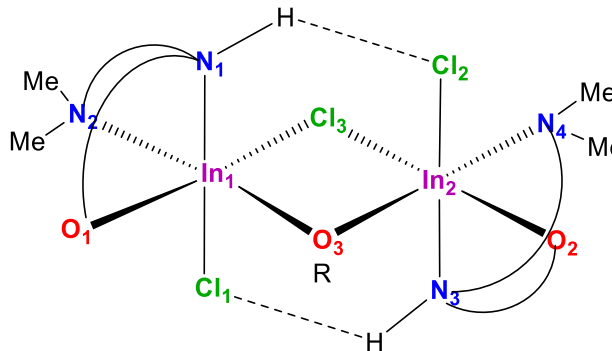


**Figure S31.** Molecular structure of  $[(\text{NNO})\text{InCl}]_2(\mu\text{-Cl})(\kappa^2,\mu\text{-diClPh})$  (**6**) depicted with ellipsoids at 50% probability (H atoms and all solvent molecules omitted for clarity). Selected bond lengths (Å): In1-O3 2.063(2), In1-Cl2 2.6327(7), In1-O1 2.081(2), In1-O4 2.2185(19), In1-N1 2.330(3), In1-N2 2.233(3), In2-Cl1 2.4340(7), In2-Cl2 2.5933(7), In2-O2 2.094(2), In2-O4 2.247(19), In2-N3 2.361(2), In2-N4 2.247(2). Selected bond angles (deg): O4-In1-Cl2 75.75(5), O3-In1-O4 97.47(8), O4-In1-N1 160.03(8), O4-In1-N2 93.53(8), O1-In1-Cl2 169.24(6).

**Table S1.** Selected solid state structural data for indium catalysts (**A**, **2-6**)



Complex	R=	In-O3(Å)	In-Cl3 (Å)	H-Cl (Å)	N1-Cl2(Å)	O1-In-Cl3 (deg)	O3-In-O1 (deg)	N1-H-Cl2 (deg)
<b>A</b>	Et	2.112(2.129)	2.636(2.667)	2.445(2.788)	3.459(4.160)	166.8(167.0)	93.0(93.0)	163.5(131.8)
<b>2</b>	C <sub>6</sub> H <sub>4</sub> Me	2.160(2.174)	2.615(2.627)	2.682(2.914)	3.619(3.823)	171.8(171.6)	95.8(94.7)	160.4(154.8)
<b>3</b>	C <sub>6</sub> H <sub>5</sub>	2.185(2.177)	2.603(2.647)	2.746(2.836)	3.662(3.740)	170.5(169.1)	93.5(94.5)	155.8(153.9)
<b>4</b>	C <sub>6</sub> H <sub>4</sub> Br	2.186(2.196)	2.629(2.631)	2.597(2.911)	3.544(3.837)	168.7(168.7)	92.6(94.2)	158.2(154.3)
<b>5</b>	C <sub>6</sub> H <sub>4</sub> NO <sub>2</sub>	2.212(2.196)	2.612(2.622)	2.484(3.758)	3.491(3.953)	166.6(167.0)	92.5(96.9)	143.9(139.1)
<b>6</b>	C <sub>13</sub> H <sub>11</sub> O <sub>2</sub> Cl <sub>2</sub>	2.219(2.248)	2.633(2.593)	2.491(NA)	3.341(NA)	169.3(173.8)	95.0(98.9)	144.2(NA)

Values in parentheses are from the second half of the molecule in non-symmetric structures.

**Table S2.** Selected crystallographic parameters

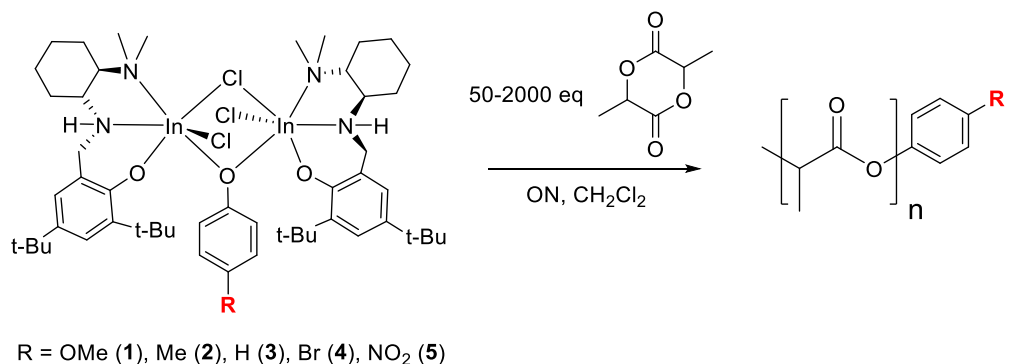
	<b>2</b>	<b>3</b>	<b>4</b>	<b>5</b>	<b>6</b>
Empirical formula	C <sub>60</sub> H <sub>93</sub> Cl <sub>3</sub> In <sub>2</sub> N <sub>4</sub> O <sub>3</sub>	C <sub>69.5</sub> H <sub>103</sub> Cl <sub>3</sub> In <sub>2</sub> N <sub>4</sub> O <sub>3</sub>	C <sub>69.5</sub> H <sub>102</sub> BrCl <sub>3</sub> In <sub>2</sub> N <sub>4</sub> O <sub>3</sub>	C <sub>106</sub> H <sub>167</sub> Cl <sub>12</sub> In <sub>4</sub> N <sub>10</sub> O <sub>10</sub> <sub>5</sub>	C <sub>73</sub> H <sub>102</sub> Cl <sub>4</sub> In <sub>2</sub> N <sub>4</sub> O <sub>4</sub>
Formula weight	1254.37	1378.54	1457.44	2634.80	1471.02
T (K)	90(2)	90(2)	90(2)	90(2)	100(2)
a (Å)	18.461(5)	17.272(2)	18.451(2)	17.446(2)	10.5118(4)
b (Å)	20.588(5)	21.834(3)	21.673(3)	18.137(2)	24.3030(10)
c (Å)	19.118(5)	18.317(2)	18.847(2)	21.873(3)	30.4559(11)
α (deg)	90	90	90	111.592(3)	90
β (deg)	110.389(4)	95.278(2)	111.583(3)	102.906(3)	93.687(2)
γ (deg)	90	90	90	98.059(3)	90
Volume (Å <sup>3</sup> )	6811(3)	6878.2(15)	7008.2(15)	6081.0(14)	7764.4(5)
Z	4	4	4	2	4
Crystal system	monoclinic	monoclinic	monoclinic	triclinic	monoclinic
Space group	P2 <sub>1</sub> /c	P2 <sub>1</sub> /c	P2 <sub>1</sub> /c	P-1	P2 <sub>1</sub> /c
d <sub>calc</sub> (g/cm <sup>3</sup> )	1.223	1.331	1.381	1.439	1.258
μ/mm <sup>-1</sup>	0.835	0.834	1.389	1.003	0.777
F(000)	2616.0	2884.0	3020.0	2715.0	3064.0
Crystal size/mm <sup>3</sup>	0.339 × 0.042 × 0.032	0.804 × 0.014 × 0.012	0.91 × 0.15 × 0.13	0.42 × 0.12 × 0.11	0.382 × 0.289 × 0.088
Radiation	MoKα (λ = 0.71073)	MoKα (λ = 0.71073)	MoKα (λ = 0.71073)	MoKα (λ = 0.71073)	MoKα (λ = 0.71073)

2Θ range for data collection/°	3.01 to 45.17	4.84 to 54.946	2.374 to 51.664	2.098 to 51.662	3.882 to 60.184
Index ranges	-19 ≤ h ≤ 19, -22 ≤ k ≤ 22, -20 ≤ l ≤ 20	-22 ≤ h ≤ 22, -28 ≤ k ≤ 27, -23 ≤ l ≤ 23	-22 ≤ h ≤ 21, -26 ≤ k ≤ 26, -17 ≤ l ≤ 23	-21 ≤ h ≤ 21, -22 ≤ k ≤ 22, -26 ≤ l ≤ 26	-14 ≤ h ≤ 14, -34 ≤ k ≤ 29, -42 ≤ l ≤ 39
Total no. reflections	30942	68285	69023	102117	69671
No. independent reflections ( $R_{int}$ )	8863 [ $R_{int} = 0.1479$ , $R_{sigma} = 0.1410$ ]	15706 [ $R_{int} = 0.0742$ , $R_{sigma} = 0.0632$ ]	13435 [ $R_{int} = 0.0652$ , $R_{sigma} = 0.0633$ ]	23130 [ $R_{int} = 0.1037$ , $R_{sigma} = 0.1151$ ]	22663 [ $R_{int} = 0.0416$ , $R_{sigma} = 0.0494$ ]
Data/restraints/parameters	8863/1089/667	15706/1542/838	13435/813/798	23130/2295/1386	22663/0/833
GOF	1.045	1.003	1.023	1.008	1.054
Final R indexes [ $I \geq 2\sigma(I)$ ]	$R_1 = 0.0882$ , $wR_2 = 0.2034$	$R_1 = 0.0410$ , $wR_2 = 0.0899$	$R_1 = 0.0493$ , $wR_2 = 0.0965$	$R_1 = 0.0544$ , $wR_2 = 0.0944$	$R_1 = 0.0489$ , $wR_2 = 0.1168$
Final R indexes [all data]	$R_1 = 0.1846$ , $wR_2 = 0.2556$	$R_1 = 0.0690$ , $wR_2 = 0.1036$	$R_1 = 0.0927$ , $wR_2 = 0.1140$	$R_1 = 0.1180$ , $wR_2 = 0.1131$	$R_1 = 0.0608$ , $wR_2 = 0.1217$
Largest diff. peak/hole / e Å <sup>-3</sup>	1.57/-1.17	1.26/-1.21	3.05/-2.07	1.39/-1.75	1.77/-0.51

a  $R1 = \sum ||Fo| - |Fc|| / \sum |Fo|$ ; b  $wR2 = [\sum(w(Fo2 - Fc2)^2) / \sum w(Fo2)^2]^{1/2}$ .

### C. Living ring-opening polymerization of lactide using catalysts 1-5

**Scheme S1.** Living ring-opening polymerization of *rac*-lactide with complexes **1-5**.



R = OMe (**1**), Me (**2**), H (**3**), Br (**4**), NO<sub>2</sub> (**5**)

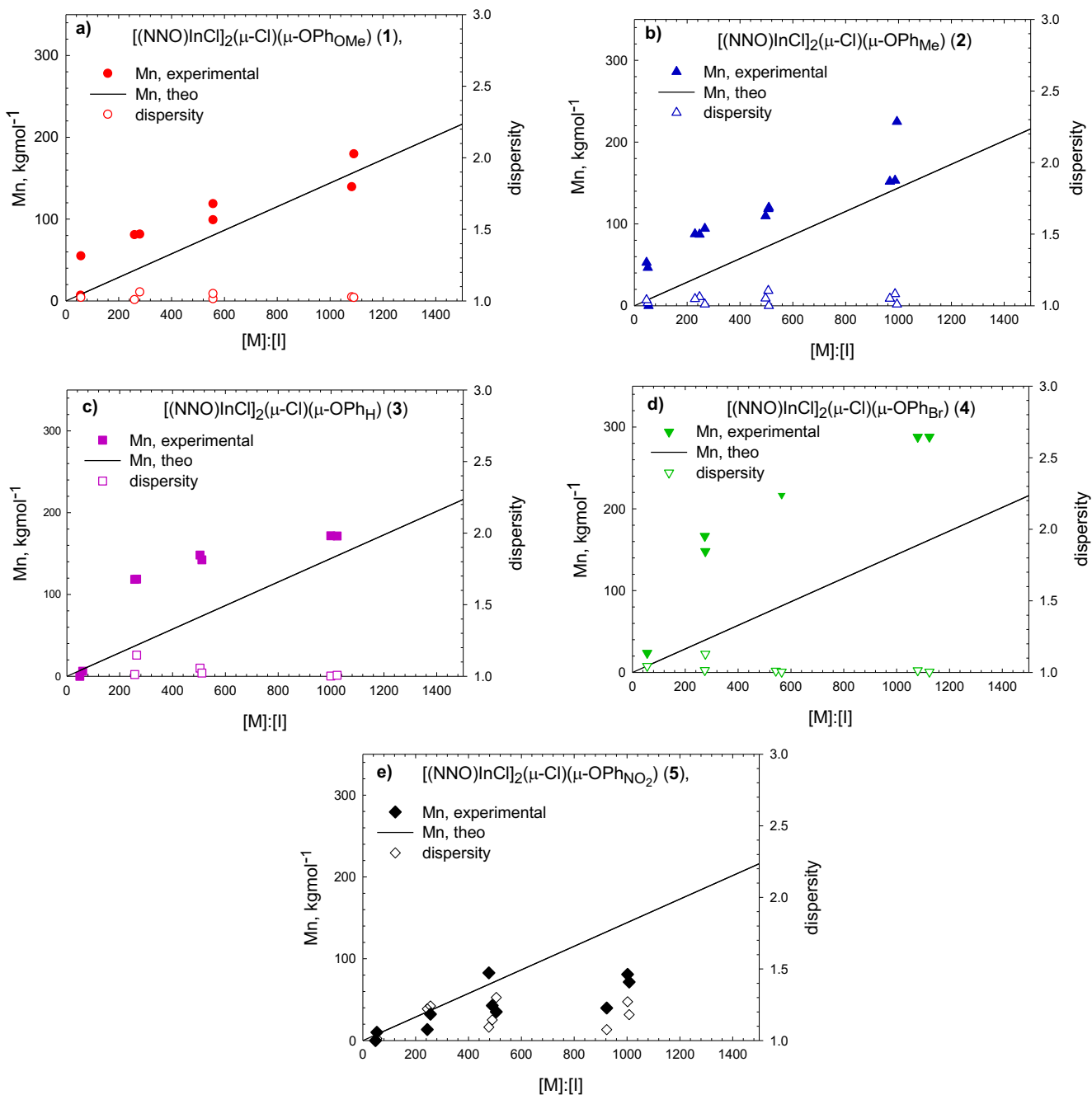


**Figure S32.** Plots of observed PLA  $M_n$  (closed symbols) and dispersity (open symbols) as functions of added *rac*-LA for a)  $[(\text{NNO})\text{InCl}]_2(\mu\text{-Cl})(\mu\text{-OPh}_{\text{OMe}})$  (1), b)  $[(\text{NNO})\text{InCl}]_2(\mu\text{-Cl})(\mu\text{-OPh}_{\text{Me}})$  (2), c)  $[(\text{NNO})\text{InCl}]_2(\mu\text{-Cl})(\mu\text{-OPh}_{\text{H}})$  (3), d)  $[(\text{NNO})\text{InCl}]_2(\mu\text{-Cl})(\mu\text{-OPh}_{\text{Br}})$  (4), and e)  $[(\text{NNO})\text{InCl}]_2(\mu\text{-Cl})(\mu\text{-OPh}_{\text{NO}_2})$  (5). ( $M_n$  = number averaged molecular weight). The line represents theoretical  $M_n$  values based on the LA:initiator ratio at 100% conversion. All reactions were carried out at room temperature in  $\text{CH}_2\text{Cl}_2$ .

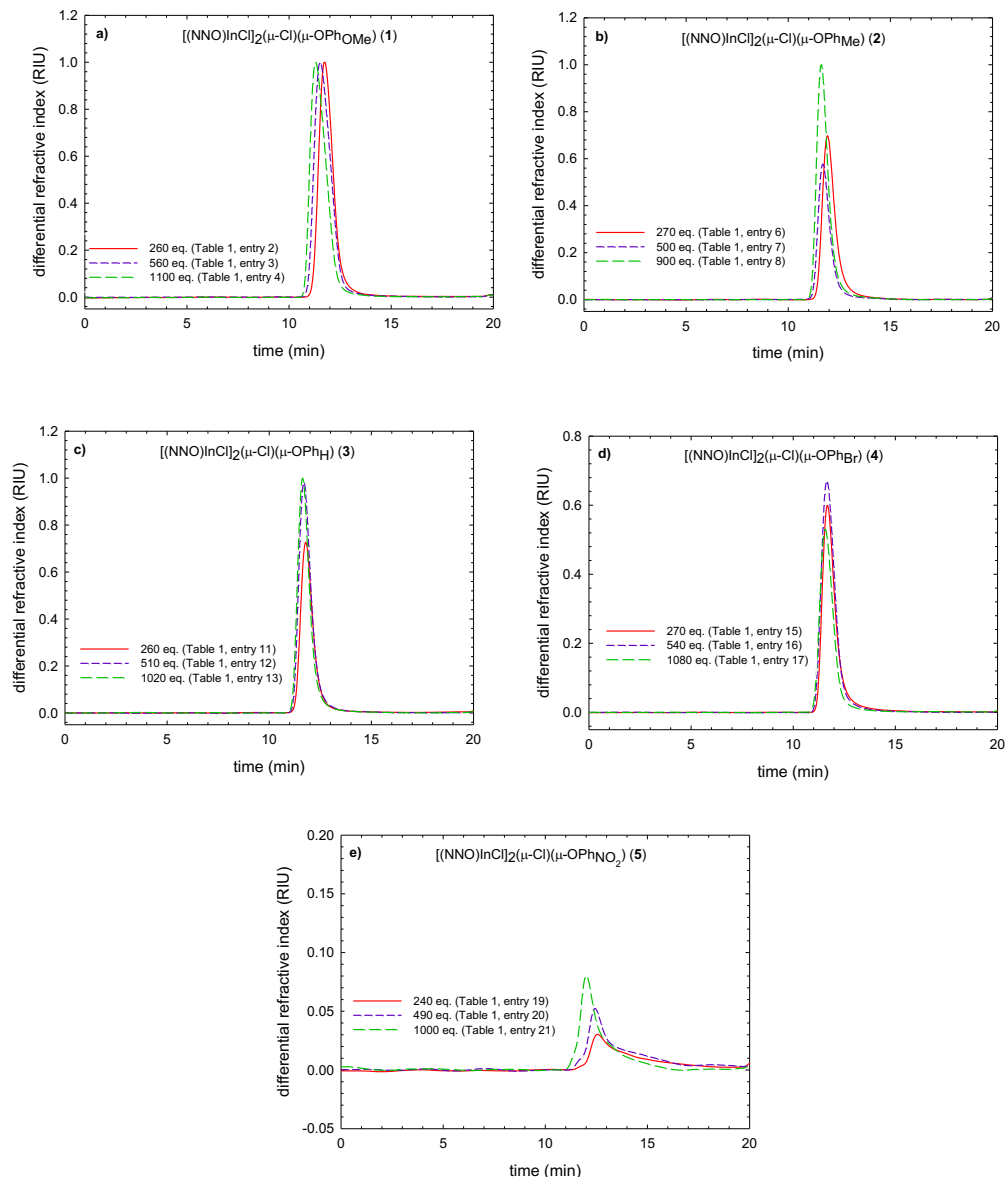


**Figure S33.** GPC traces for the living polymerization of *rac*-lactide for complexes: a)  $[(\text{NNO})\text{InCl}]_2(\mu\text{-Cl})(\mu\text{-OPh}_{\text{OMe}})$  (1), b)  $[(\text{NNO})\text{InCl}]_2(\mu\text{-Cl})(\mu\text{-OPh}_{\text{Me}})$  (2), c)  $[(\text{NNO})\text{InCl}]_2(\mu\text{-Cl})(\mu\text{-OPh}_\text{H})$  (3), d)  $[(\text{NNO})\text{InCl}]_2(\mu\text{-Cl})(\mu\text{-OPhBr})$  (4), e)  $[(\text{NNO})\text{InCl}]_2(\mu\text{-Cl})(\mu\text{-OPhNO}_2)$  (5).

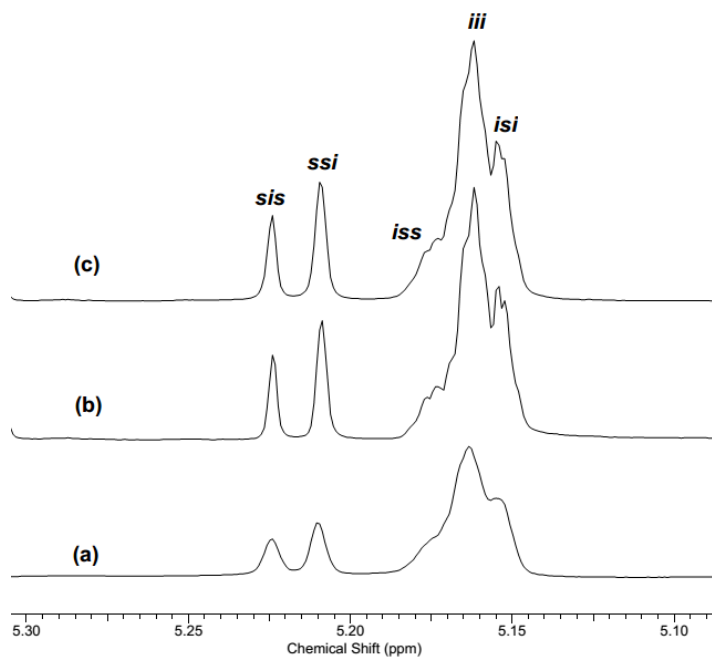


**Figure S34.**  $^1\text{H}\{^1\text{H}\}$  NMR ( $\text{CDCl}_3$ , 25 °C) spectrum of the methylene region of polymers generated from a)  $(\pm)$ - $[(\text{NNO})\text{InCl}]_2(\mu\text{-Cl})(\mu\text{-OEt})$  (**A**), b)  $(\pm)$ - $[(\text{NNO})\text{InCl}]_2(\mu\text{-Cl})(\mu\text{-OPhOMe})$  (**1**) ( $\pm$ )- $[(\text{NNO})\text{InCl}]_2(\mu\text{-Cl})(\mu\text{-OPh})$  (**3**). All these polymers show the same distribution of tetrad peaks implying the same stereocontrol mechanism is acting in all the systems.

#### D. Chain-end fidelity

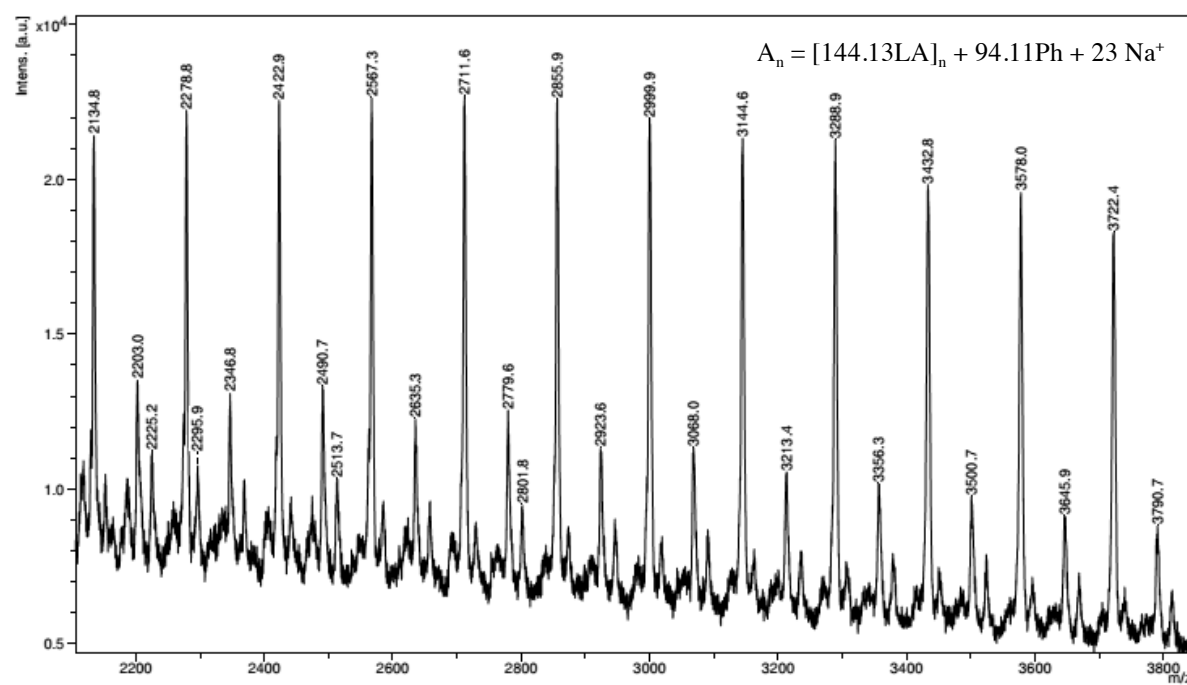
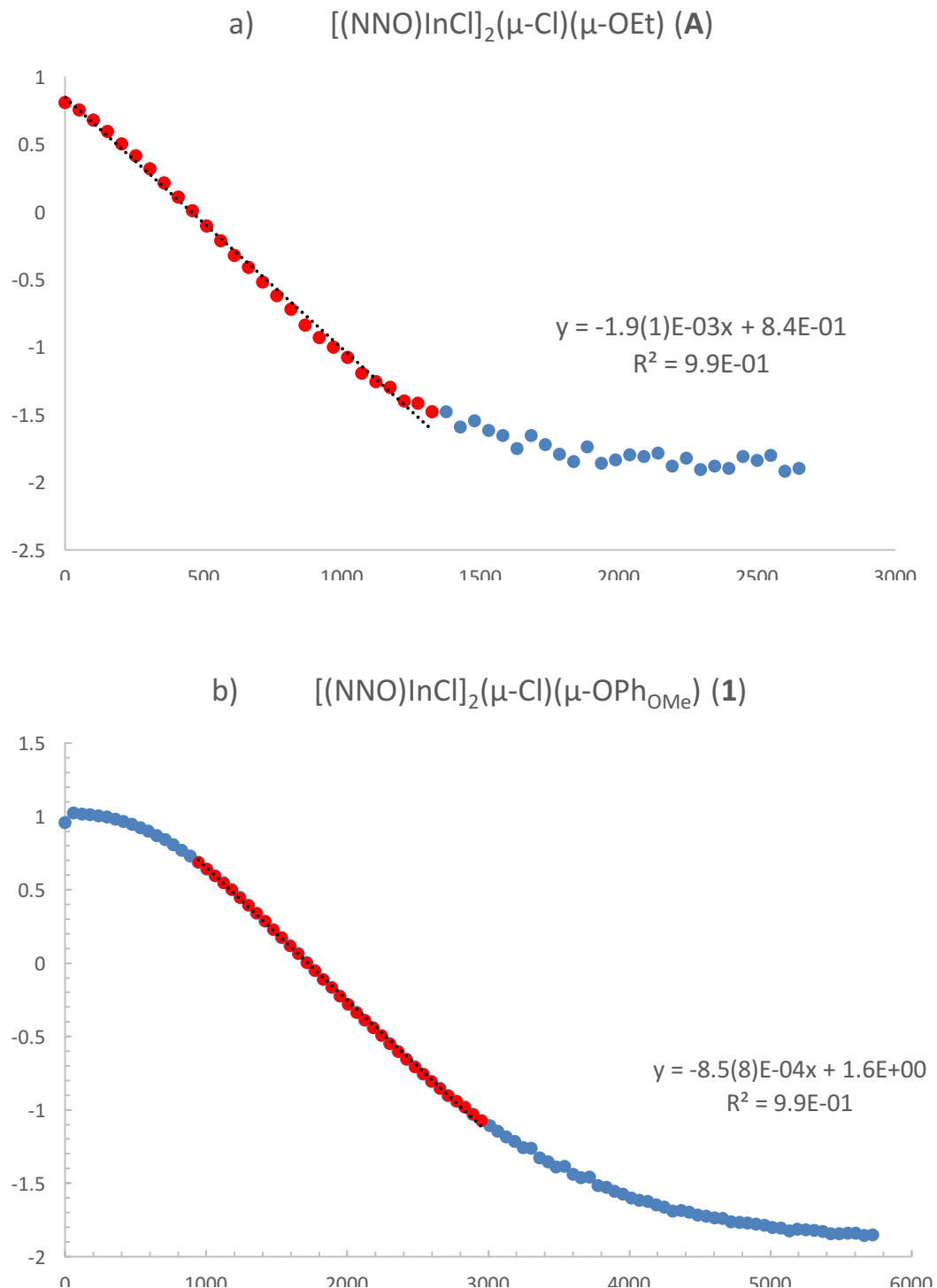
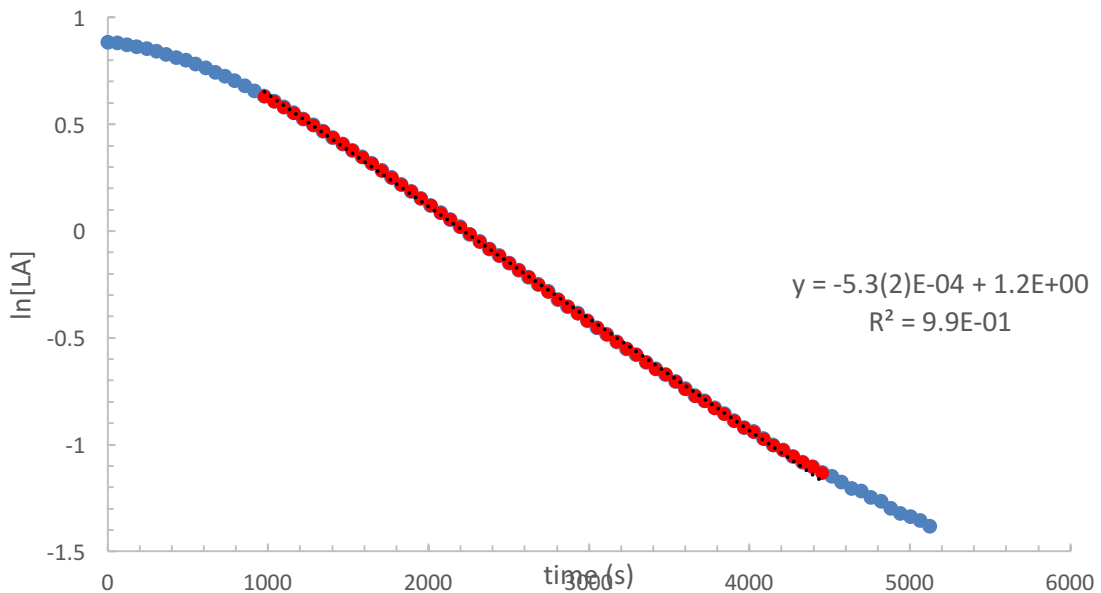


**Figure S35.** MALDI-TOF spectrum from polymerization of [LA]:[3] with ratios of 49:1 (Table 1 entry 10).

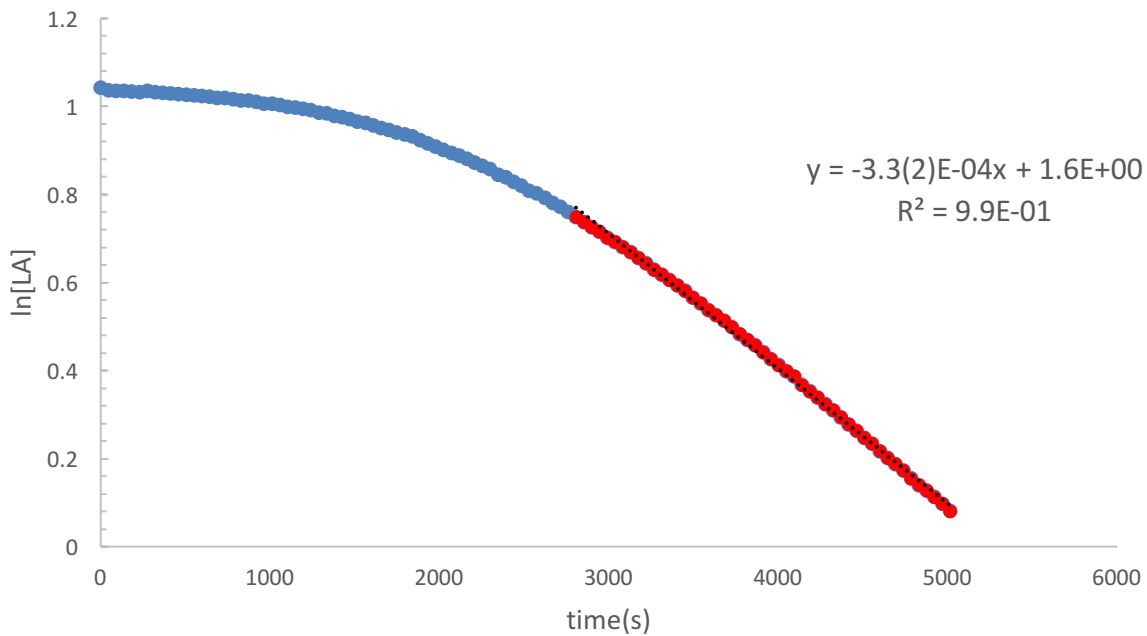
**E. In situ living ring-opening polymerization data with catalysts 1-4.**



c)  $[(\text{NNO})\text{InCl}]_2(\mu\text{-Cl})(\mu\text{-OPh}_{\text{Me}})$  (**2**)



d)  $[(\text{NNO})\text{InCl}]_2(\mu\text{-Cl})(\mu\text{-OPh}_\text{H})$  (**3**)



e)  $[(\text{NNO})\text{InCl}]_2(\mu\text{-Cl})(\mu\text{-OPh}_{\text{Br}})$  (**4**)

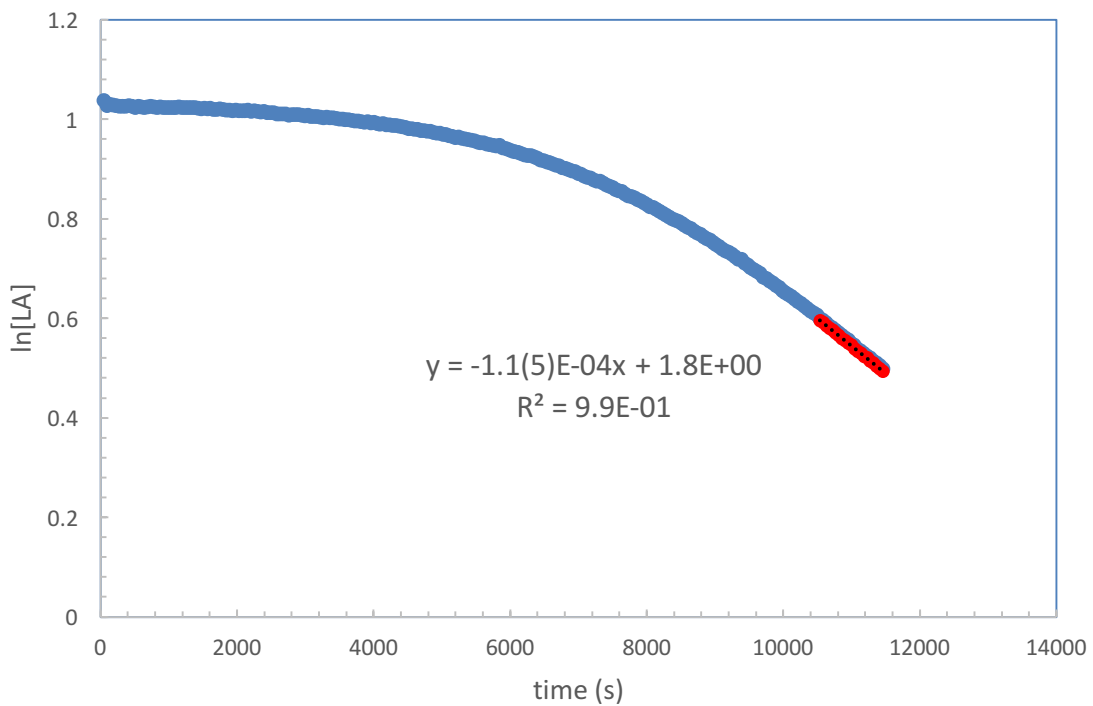
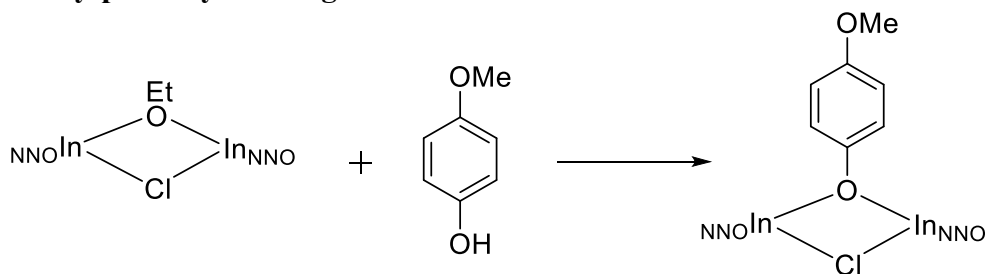
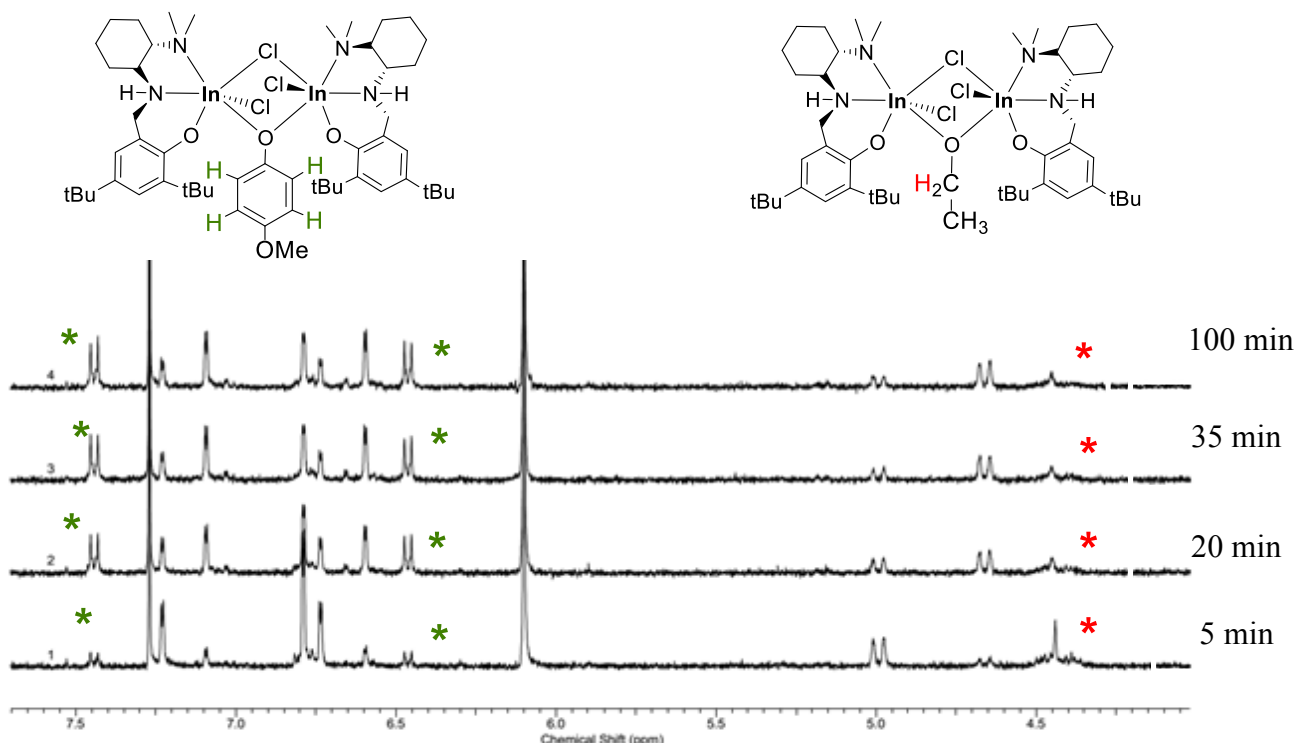


**Figure S36.** Reactions were carried out in an NMR tube at 25 °C. 1,3,5-trimethoxybenzene (TMB) was used as internal standard. All reactions were carried out with 50 equivalents of LA in CD<sub>2</sub>Cl<sub>2</sub> at 25 °C and followed by <sup>1</sup>H NMR spectroscopy. a) [A] = 0.0046 M, [LA] = 0.22 M. b) [1] = 0.0039 M, [LA] = 0.19 M. c) [2] = 0.0043 M, [LA] = 0.21 M. d) [3] = 0.0037 M, [LA] = 0.22 M. e) [4] = 0.0041 M, [LA] = 0.22 M. The value of  $k_{obs}$  was determined from the slope of ln[LA] vs. time (shown in red), averaged from at least three experiments.

## F. Alkoxy-phenoxy exchange kinetics

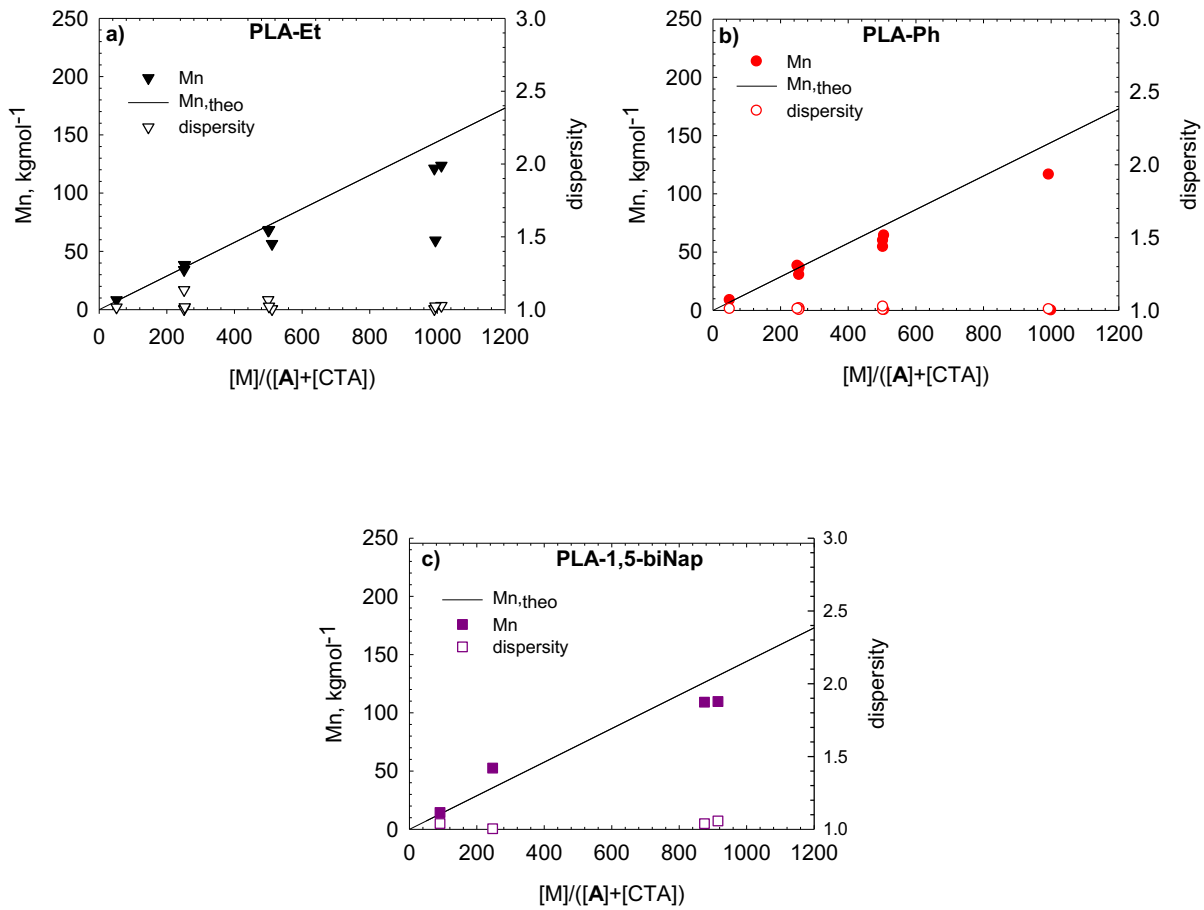


**Scheme S2.** Alkoxy-phenoxy exchange reaction with complex **A** and para-methoxy phenol.

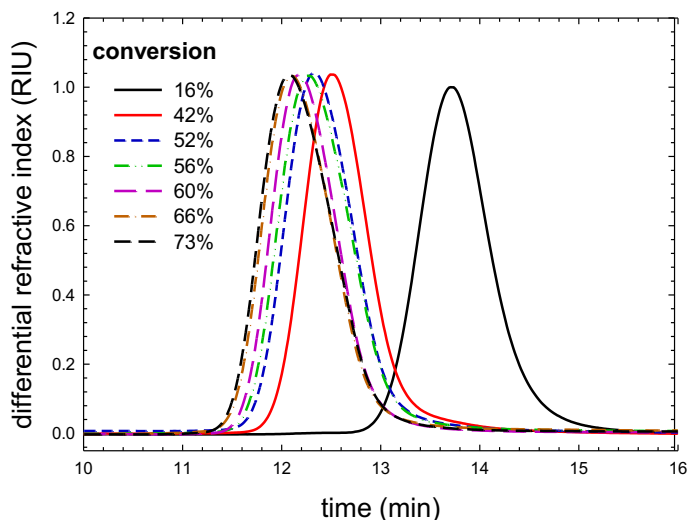


**Figure S37.**  $^1\text{H}$  NMR ( $\text{CD}_2\text{Cl}_2$ , 25 °C) spectrum of the alkoxy-phenoxy exchange reaction with complex **A** and para-methoxy phenol. The loss of the bridging ethoxy peaks (denoted by red stars) and the emergence of bridging phenoxy signals (denoted by green stars) were monitored and used to calculate the rate of exchange,  $k_{\text{exchange}}$ .

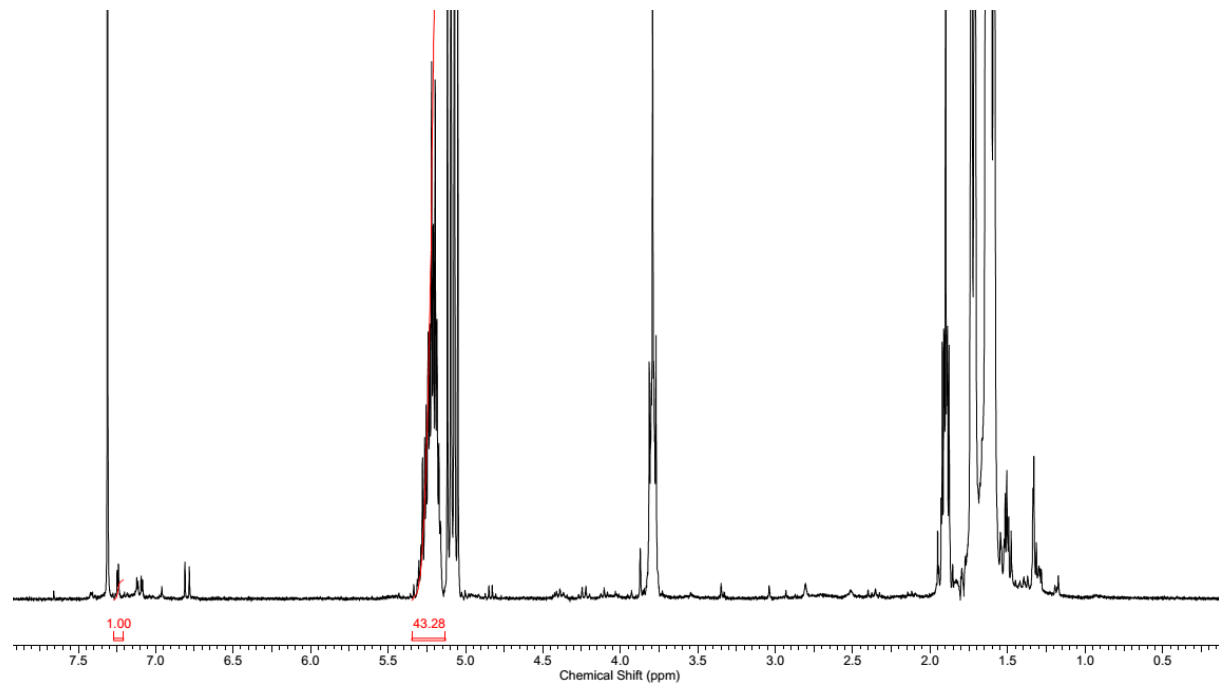
## G. Immortal ring-opening polymerization data



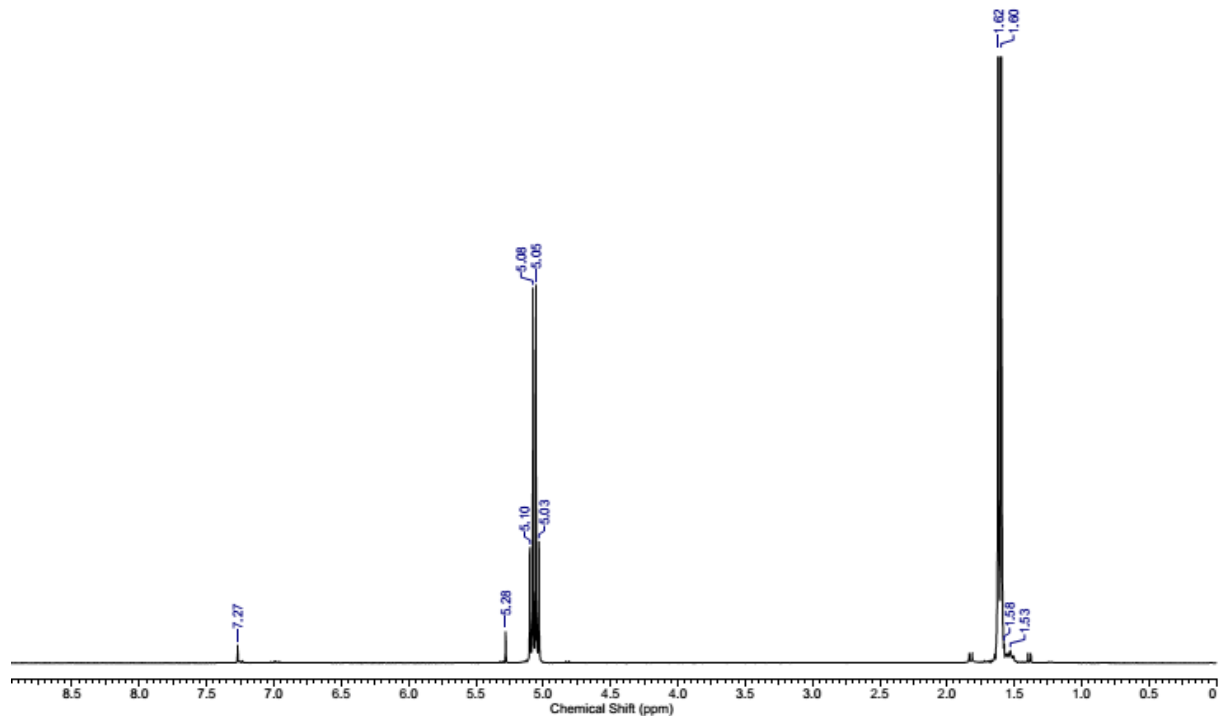
**Figure S38.** Plots of observed PLA  $M_n$  (closed symbols) and dispersity (open symbols) as functions of  $[LA]:([A]+[CTA])$  for (a) CTA = ethanol (PLA-Et), (b) CTA = phenol (PLA-Ph), (c) CTA = 1,5-naphthalenediol (PLA-1,5-Nap).



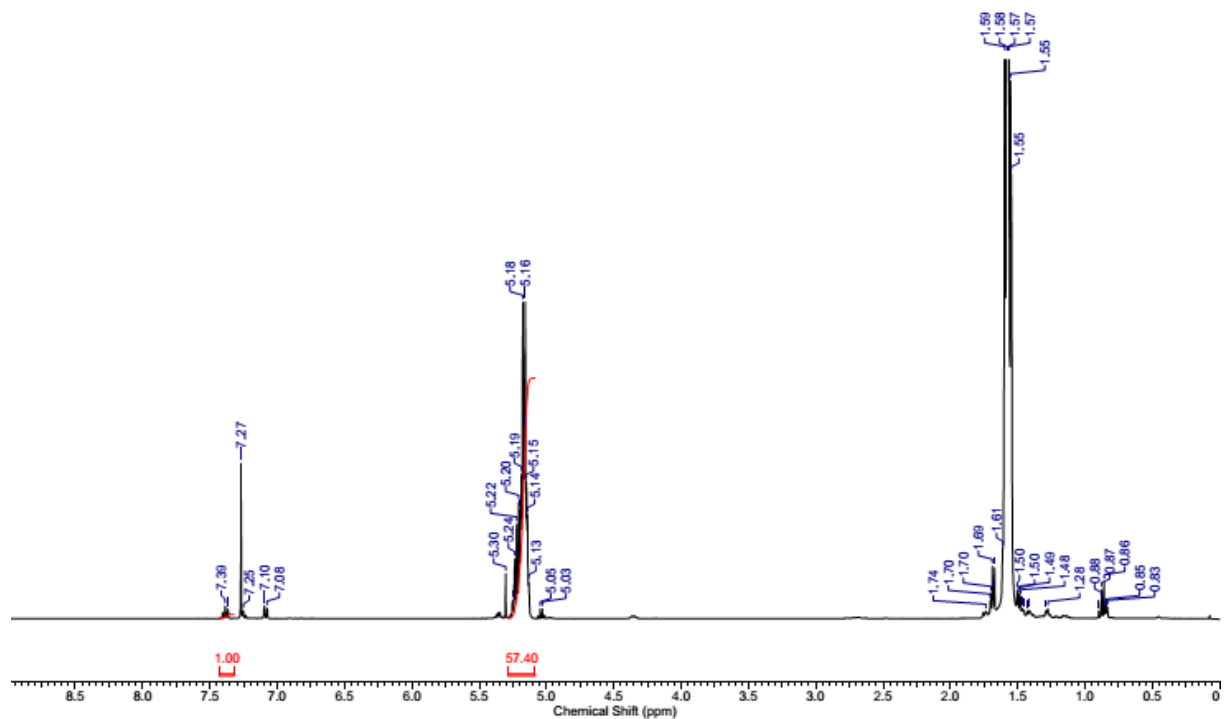
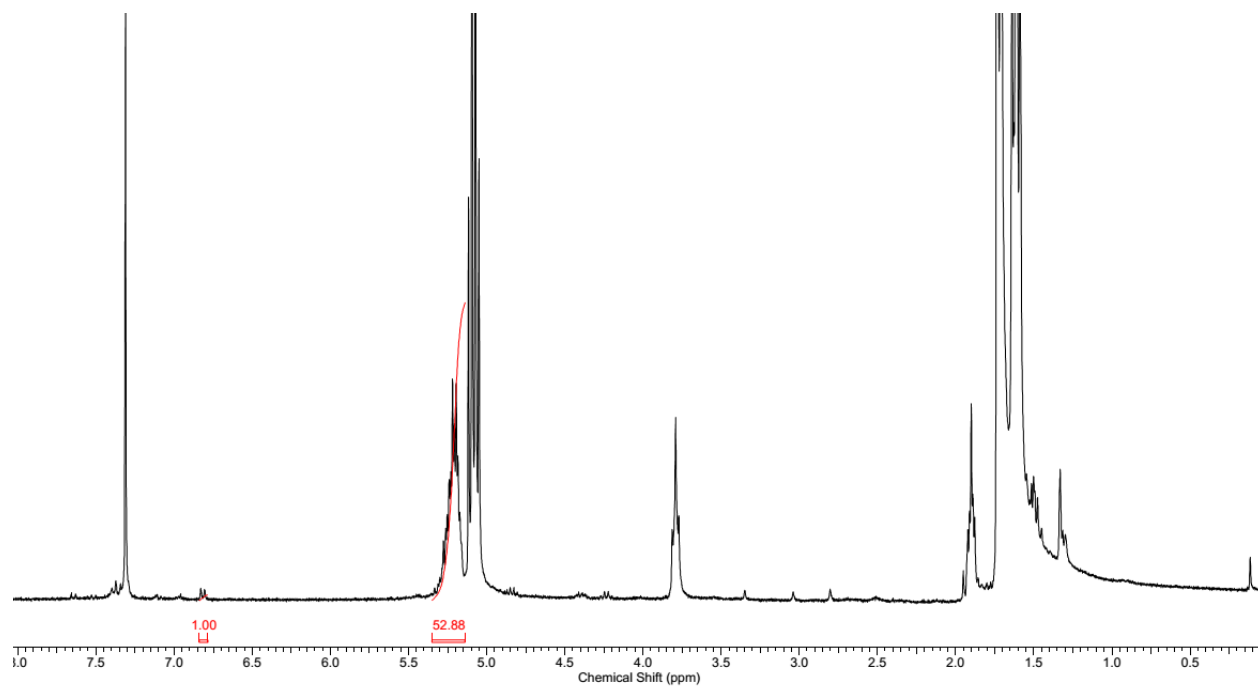
**Figure S39.** GPC traces with respect to conversion for the immortal polymerization of lactide with **A** with phenol ([LA]:[A]:[phenol] = 10500:1:20).



**Figure S40.**  $^1\text{H}$  NMR ( $\text{CDCl}_3$ , 25 °C) spectrum of PLA isolated from polymerization of [LA]:[diClPh]:[A] ratios of 237:2:1 (Table S3, entry 2).



**Figure S41.**  $^1\text{H}$  NMR ( $\text{CDCl}_3$ , 25 °C) spectrum of PLA isolated from polymerization of [LA]:[biPhen]:[A] ratios of 583:10:1 (Table S3, entry 3).



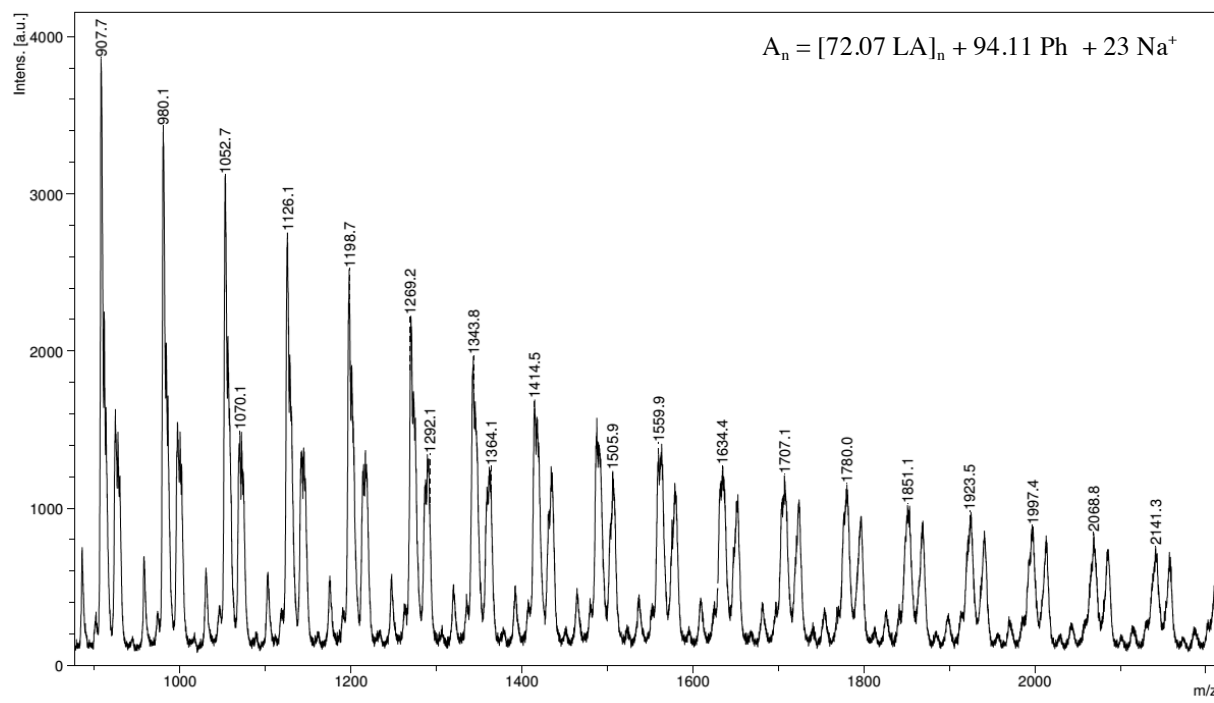


**Figure S44.** MALDI-TOF spectrum for a selected PLA-Ph sample.

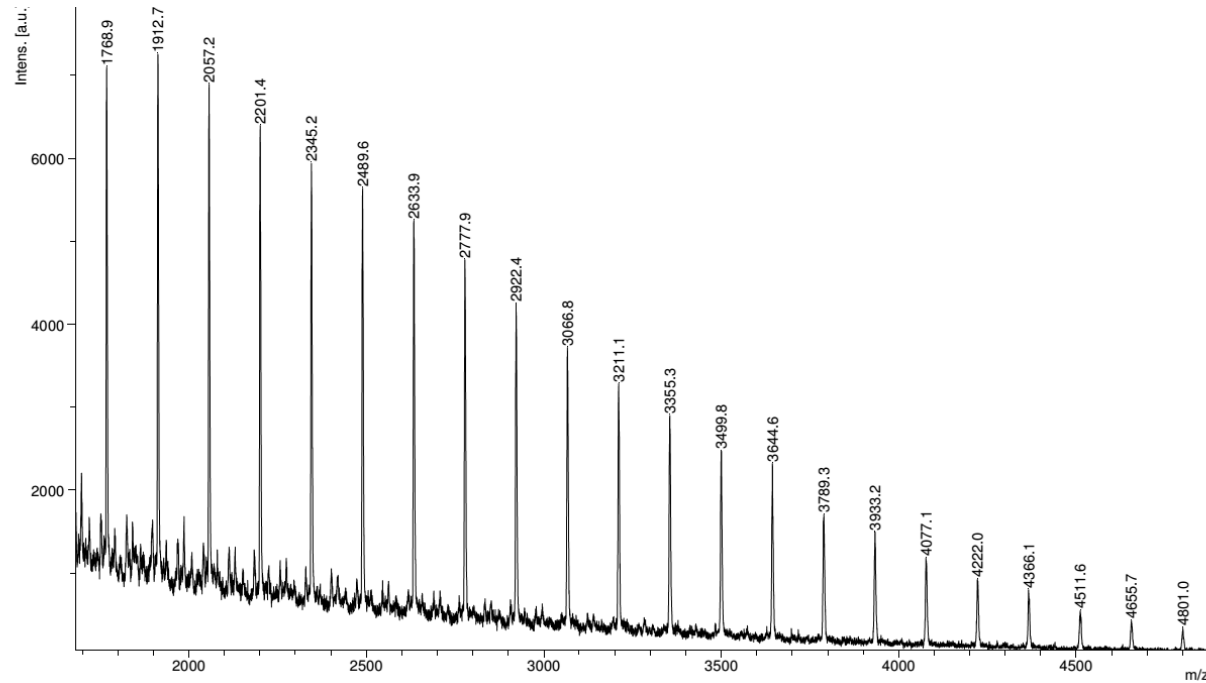


**Figure S45.** MALDI-TOF spectra for a) a selected PLA-1,5-Nap sample.

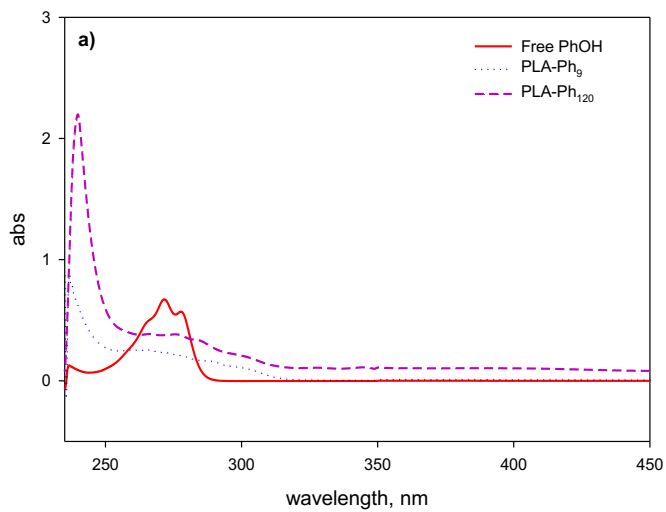


**Figure S46.** Solution UV-Vis spectra for a) PLA-Ph. Polymer solutions were in  $\text{CHCl}_3$  with an end-group concentration of 0.0003M.

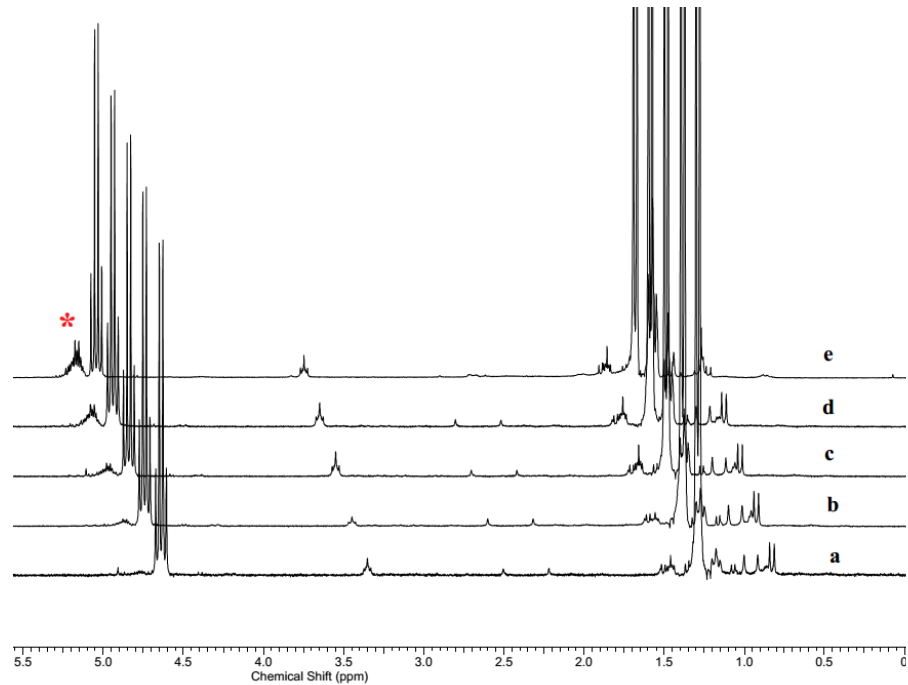


**Figure S47.**  $^1\text{H}$  NMR ( $\text{CDCl}_3$ , 25 °C) spectrum of polymerization  $[\text{LA}]:[6] = 110$  in THF. a) 15 hours, b) 24 hours, c) 48 hours, d) 72 hours, e) 120 hours. Red star shows polymer signal.

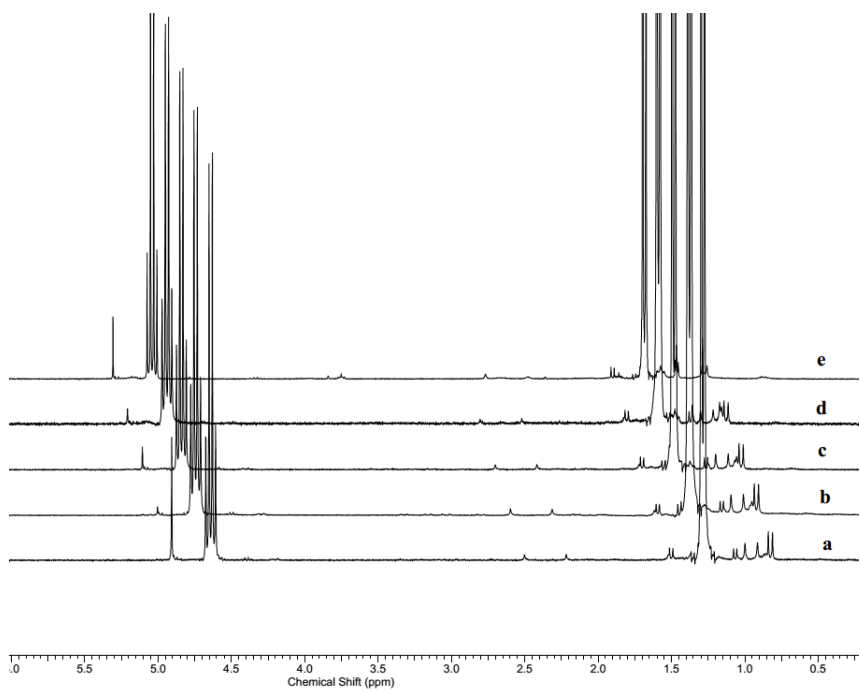


**Figure S48.** <sup>1</sup>H NMR ( $\text{CDCl}_3$ , 25 °C) spectrum of polymerization  $[\text{LA}]:[6] = 110$  in dichloromethane. a) 15 hours, b) 24 hours, c) 48 hours, d) 72 hours, e) 120 hours.